

Crustal channel flows: 2. Numerical models
with implications for metamorphism in the Himalayan-Tibetan Orogen

Rebecca A. Jamieson¹, Christopher Beaumont², Sergei Medvedev^{2,3}, and Mai H. Nguyen^{1,2}

¹Department of Earth Sciences, Dalhousie University, Halifax, N.S., Canada B3H 3J5

²Department of Oceanography, Dalhousie University, Halifax, N.S., Canada B3H 4J1

³Present address: Freie Universitat Berlin, Fachrichtung Geologie, Malteserstrasse 74-100,
D-12249 Berlin, Germany

Paper submitted to *Journal of Geophysical Research*, 23 September, 2003

Accepted pending revision, 25 February, 2004; revised version accepted 16 March, 2004.

File name: 2003JB002811_Text.doc

Abstract

Results from a thermal-mechanical model (HT1) that includes mid-crustal channel flow are compatible with many features of the Himalayan-Tibetan system. Radioactive self-heating and rheological weakening of thickened model orogenic crust lead to the formation of a hot, low-viscosity mid-crustal channel and a broad plateau. Channel material, corresponding to the Greater Himalayan Sequence (GHS), flows outward from beneath the plateau in response to topographically-induced differential pressure. At the plateau flank it is exhumed by focused surface denudation and juxtaposed with cooler, newly accreted material corresponding to the Lesser Himalayan Sequence (LHS). The model channel is bounded by coeval thrust- and normal-sense ductile shear zones, interpreted to represent the Main Central Thrust (MCT) zone and South Tibetan Detachment (STD) system respectively. Inverted metamorphism associated with the model MCT zone results from distributed ductile shear along the MCT and extrusion of the hot channel. A variety of model P - T - t path styles, resembling those observed in the GHS and LHS, are produced for points traveling through contrasting tectonic regimes that coexist in different parts of the model. Predicted times of peak metamorphism, cooling, and erosion of metamorphic facies are generally compatible with observations, although model GHS cooling ages are too young. The times of M1 and M2 metamorphic 'events' observed in the GHS correspond to model times of maximum burial and maximum heating respectively. The results highlight the need to integrate tectonics and metamorphism in continental collision models, and demonstrate the importance of lateral transport of both heat and material in large hot orogens.

Key words: thermal-mechanical models, channel flow, Himalayan-Tibetan orogen, P - T - t paths, inverted metamorphism, ductile extrusion, crustal tectonics

1. Introduction

Quantitative models for the thermal and tectonic evolution of orogenic belts [e.g., *Oxburgh and Turcotte*, 1970; *England and Thompson*, 1984; *Ruppel and Hodges*, 1994; *Huerta et al.*, 1998] have strongly influenced the ways in which metamorphic geologists interpret their observations in terms of tectonic processes. In particular, model results are used to interpret pressure-temperature-time (*P-T-t*) paths, constructed from a range of petrological and thermochronological data, in terms of particular tectonic styles [e.g., *Spear*, 1993; and references therein]. Among the various problems to which this approach has been applied, none has attracted more attention than the relationship between metamorphism and continental collision in the Himalayan-Tibetan system. Many numerical and conceptual models have been proposed to account for certain aspects of the metamorphic and tectonic history of this region, notably the origin of the 'inverted' metamorphism associated with the Main Central Thrust zone [e.g., *LeFort*, 1975; *Searle and Rex*, 1989; *Molnar and England*, 1990; *Royden*, 1993; *Henry et al.*, 1997; *Harrison et al.*, 1998; *Huerta et al.*, 1999]. The challenge is to produce an internally consistent, quantitative model that not only explains the petrological observations, but is also compatible with the tectonic evolution and geometry of the orogen as a whole.

Coupled thermal-mechanical numerical models designed to investigate the metamorphic and tectonic evolution of convergent orogens [e.g., *Jamieson et al.* 1996, 1998; *Batt and Braun*, 1997], have recently been applied to the Himalayan-Tibetan system [*Beaumont et al.*, 2001a,b; *Koons et al.*, 2002]. These models predict interactions between heat and material transfer in an internally consistent manner, and can be used to calculate crustal deformation and exhumation histories, thermal evolution, and the resulting metamorphic response, including *P-T-t* paths. *Beaumont et al.* [2001a, 2004] showed that models incorporating a set of thermally and tectonically coupled processes, including crustal thickening, rheological weakening in the middle

crust beneath Tibet, mid-crustal channel flow, and focused surface denudation, are compatible with a wide range of observations from the Himalayan-Tibetan system [e.g., *Searle*, 1996; *Hodges*, 2000, *DeCelles et al.*, 2002; *Haines et al.*, 2003]. In particular, channel flow models provide an internally consistent explanation for coeval north-south shortening on the Main Central Thrust (MCT) system and north-south extension along the South Tibetan Detachment (STD) system, high-grade metamorphism and anatexis in the Greater Himalayan sequence (GHS), 'inverted' metamorphism within the MCT zone and subjacent Lesser Himalayan sequence (LHS), and the formation of gneiss domes in southern Tibet [*Beaumont et al.*, 2001a].

The purpose of this paper is to test the plausibility of a representative channel flow model (HT1; similar but not identical to Model 3 of *Beaumont et al.*, 2001a) by comparing its thermal and metamorphic evolution with various types of metamorphic and geochronologic data from the Himalaya. The tectonic evolution of the same model is described in a companion paper [*Beaumont et al.*, 2004]. We also explore the implications of the model results for metamorphic processes in the Himalaya and elsewhere, including the origin of the inverted metamorphism, the tectonic significance of certain *P-T-t* path styles, and the role of continuous vs. discrete metamorphic events. In particular, the results point to the importance of lateral transport of heat and material in large, hot orogens like the Himalayan-Tibetan system.

2. Model design

Model HT1 (Fig. 1; Table 1) is an advancing subduction model with a three-layer crust and focused surface denudation. This is one of a series of related models [e.g., *Beaumont et al.*, 2001a,b, 2004] that display features relevant to the metamorphic and tectonic evolution of the Himalayan-Tibetan system. Model HT1 was selected because its tectonic evolution is relatively simple and broadly compatible with first-order features observed along the 2000 km length of the

orogen [e.g., *Hodges, 2000*]; no attempt was made to adjust model parameters to match specific transects or metamorphic datasets. Boundary conditions, initial configuration, and other parameters used in HT1 are given in Fig. 1 and Table 1. A more extensive discussion of the choice of boundary conditions and sensitivity to key parameters is presented in *Beaumont et al. [2004]*. The model was run for 54 My, since most workers agree that the main Himalayan collision began at 50-55 Ma [e.g., *Searle, 1996; Hodges, 2000*]. Specific features of this model that control its metamorphic evolution are discussed briefly below.

2.1. Tectonic style

The model is driven by subduction of sub-orogenic lithosphere (Fig. 1). Pro-crust and mantle lithosphere advance at velocity V_P on stationary retro-crust and mantle ($V_R = 0$), and detach and subduct at point S [*Willett et al., 1993*]. In model HT1, $V_P = 5$ cm/y is partitioned between S-point (subduction) advance at $V_S = 2.5$ cm/y and subduction at $V_P - V_S = 2.5$ cm/y (Fig. 1). This limits the retro-ward translation of the model suture, so that its final position lies between the erosion front and the underlying S-point [*Beaumont et al., 2001a, 2004*], and also limits the cooling effect from the downgoing slab. Advance of the S-point is accommodated by kinematic ablative subduction of the retro-mantle [Fig. 1; cf. *Pope and Willett, 1998*]; fully coupled thermal-mechanical calculations are limited to the model crust. Subduction advance and other aspects of mantle dynamics do not have a significant effect on the model behavior in the vicinity of the orogenic front because the weak lower crust becomes decoupled from the underlying mantle tectonics [*Beaumont et al., 2001b, 2004*].

Model HT1 has three crustal layers with contrasting thermal and mechanical properties (Fig. 1; Table 1). The upper crust (0-10 km) has a "wet quartzite" (WQ) rheology [*Gleason and Tullis, 1995*], the middle crust (10-25 km) has the same rheology with B^* increased by a factor of 5 (WQx5), and the lower crust (25-35 km) has a "dry Maryland diabase" (DMD) rheology

[Mackwell *et al.*, 1998]. For the upper crust (0-10 km) $\phi_{eff} = 5^\circ$ and for the middle and lower crust (10-35 km) $\phi_{eff} = 15^\circ$. The model orogen is made up of thickened middle and upper crust [cf. DeCelles *et al.*, 2002]. The strong lower crust is subducted and does not influence the tectonic evolution of the system except for its effect on the properties of incoming pro-lithosphere. In contrast, the tectonic style of the model orogen is very sensitive to the mechanical properties of the weak upper crust [Beaumont *et al.*, 2001a, 2004].

An essential component of the rheological model is an extra increment of temperature-dependent viscosity reduction in the middle and upper crustal layers beyond that predicted by the flow laws. Between 700° and 750°C , corresponding broadly to the temperature range for muscovite dehydration melting, the effective viscosity is reduced linearly from its flow law value at 700°C to 10^{19} Pa.s at $T \geq 750^\circ\text{C}$ [Fig. 1; Beaumont *et al.*, 2001a; 2004]. The resulting effective viscosity is reduced by a factor of about 5-50; this is probably a conservative estimate for the viscosity reduction attributable to the presence of a small amount of *in situ* partial melt [e.g., Rushmer, 2001; Mecklenburgh and Rutter, 2003]. For convenience, we refer to this as 'melt weakening' [Beaumont *et al.*, 2001a; Jamieson *et al.*, 2002], since there is abundant field evidence from the GHS that melt was present during much of its deformation history [e.g., Hollister, 1993; Hodges *et al.*, 1993; Davidson *et al.*, 1997; Coleman, 1998; Grujic *et al.*, 2002]. However, any other geological process producing a comparable reduction in effective viscosity over the same temperature range would have a similar effect in the model.

2.2. Heat source

A number of different heat sources have been proposed to account for Himalayan metamorphism, including radiogenic heating from thickened and/or underplated crustal material [e.g., Royden, 1993; Huerta *et al.*, 1998], heat from the asthenosphere via removal of sub-

orogenic mantle lithosphere and/or slab break-off [e.g., *Molnar et al.*, 1993; *Mahéo et al.*, 2002], and strain heating associated with dissipation of mechanical energy on the MCT [e.g., *Molnar and England*, 1990; *England and Molnar*, 1993; *Harrison et al.*, 1998]. Model HT1 relies mainly on radiogenic heat production from thickened orogenic crust, and thus represents one end member in a spectrum of possible thermal-tectonic styles.

Model calculations include the effects of thermal diffusion, heat advection, and radioactive heat production [Table 1; *Jamieson et al.*, 2002; *Beaumont et al.*, 2004]. In model HT1, heat production in the upper crust is $2.0 \mu\text{W}/\text{m}^3$ (A_1 ; 0-20 km), and in the lower crust is $0.75 \mu\text{W}/\text{m}^3$ (A_2 ; 20-35 km), which are considered reasonable values for continental margin crust like that interpreted to make up most of the Himalayan-Tibetan orogen south of the Indus-Tsangpo suture [e.g., *Huerta et al.*, 1998, 1999; *DeCelles et al.*, 2002]. In particular, upper crustal heat production (A_1) lies within the range of measured values from the Himalaya [ca. 1.5 to $> 6 \mu\text{W}/\text{m}^3$; *Huerta et al.*, 1999, and references therein]. The combination of these values with the basal mantle heat flux (q_m) of $20 \text{ mW}/\text{m}^2$ leads to an initial Moho temperature of 704°C and an initial surface heat flux (q_s) of $71.25 \text{ mW}/\text{m}^2$ (Fig. 1).

2.3. Exhumation mechanism

The most effective mechanisms for rapidly exhuming metamorphic rocks are syn-orogenic erosion and normal faulting [e.g., *Ring et al.*, 1999]. These processes are well documented in the Himalaya and have been used to explain metamorphic P - T - t paths and thermochronological data from the orogen and its foreland [e.g., *Burg et al.*, 1984; *Copeland and Harrison*, 1990; *Burchfiel et al.*, 1992; *France-Lanord et al.*, 1993; *Hodges et al.*, 1993; *Edwards and Harrison*, 1997; *Zeitler et al.*, 2001; *Koons et al.*, 2002]. It is widely recognized that coeval thrusting along the MCT and normal movement on the STD played a dominant role in exhumation of the GHS [e.g., *Burchfiel and Royden*, 1985; *Searle and Rex*, 1989; *Hodges et al.*, 1992; *Hodges*, 2000].

Various conceptual and quantitative models, including extrusion of a rigid wedge or 'pip' [e.g., *Burchfiel and Royden, 1985; Hodges et al., 1993, 1996*] and ductile extrusion of an internally deforming wedge or channel [e.g., *Grujic et al., 1996; Wu et al., 1998; Vannay and Grasemann, 2001; Hodges et al., 2001; Beaumont et al., 2001a*], have been proposed to account for this process.

The dominant exhumation mechanism in model HT1 is syn-orogenic surface denudation that is focused on the pro-side of the system. Coupling between erosion at the model surface and channel flow at depth leads to ductile extrusion of a weak mid-crustal region between coeval normal- and thrust-sense shear zones [*Beaumont et al., 2001a*]. The rate of surface denudation varies with distance, time, and surface slope [*Beaumont et al., 2004*]. The space- and time-dependent denudation functions are pre-defined ($f(t)$, $g(x)$; Fig. 1, Table 1); slope is determined by the interaction of model tectonics with the imposed denudation functions. In Model HT1 there is no erosion during the plateau-building stage (0-24 My). After 24 My, slope-dependent surface denudation is focused on the flank of the orogenic plateau (details in Fig. 2). A high denudation rate, reaching a maximum of ca. 1 cm/y in the regions of highest slope, is maintained until 39 My. Denudation rate declines gradually for the last 15 My of model evolution, based on geochronological data [e.g., *White et al., 2002; Vannay et al., 2004*] indicating a reduction in GHS erosion rate at about that time. However, even at the end of the model (54 My) the erosion rate in the regions of highest slope is 1-4 mm/y (Fig. 2d), within the range of estimates from the modern orogenic front [e.g., *Burbank et al., 1996; Galy and France-Lanord, 2001; Finlayson et al., 2002*].

3. Crustal-scale thermal-tectonic evolution

Figures 2 and 3 show crustal-scale deformation, velocity field, thermal structure, and metamorphic evolution of model HT1 at four times (21, 33, 42, 54 My) relevant to comparisons with metamorphic data from the Himalayan-Tibetan system. For simplicity, only the pro-side of the model is shown. Other results from HT1 and related models are presented in *Beaumont et al.* [2004]. In the following discussion, "My" refers to millions of years since the start of the model, and "Ma" refers to millions of years before the end of the model ($\text{Ma} = 54 - \text{My}$), which is more useful for comparing model results with data. Other notation is summarized in Tables 1 and 2.

3.1. Crustal thickening and thermal evolution

At 21 My, just before the onset of erosion, model crustal thickness is near its maximum (Fig. 2a). Thickening of the radioactive upper crust has produced a significant volume of lower crust at $T > 700^\circ\text{C}$, the threshold for 'melt weakening'. The ca. 20 My time-scale for radioactive self-heating of thickened crust sufficient for partial melting is characteristic of models with the convergence rates and heat production assumed here [*Beaumont et al.*, 2004]. The presence of a low-viscosity region in the lower crust in combination with the topographic gradient causes the weak material to flow outwards toward the flank of the orogen, forming a lower crustal channel [e.g., *Royden*, 1996; *Clark and Royden*, 2000; *Beaumont et al.*, 2001a,b; *Hodges et al.*, 2001; *Jamieson et al.*, 2002]. This effect can be seen in the deformed marker grid and the velocity field in the lower crust between markers -1 and 0 (Fig. 2a). This time (21 My=33 Ma) represents an early stage of channel flow in the model, and corresponds approximately to the time of the 'Eohimalayan' (M1) metamorphism [e.g., *Hodges et al.*, 1996; *Vance and Harris*, 1999; *Simpson et al.* 2000].

By 33 My, the channel has propagated outward so that it underlies most of the pro-side of the thickened crust, leading to the formation of a wide plateau [e.g., *Medvedev et al.*, 2000;

Vanderhaeghe et al., 2003]. A large volume of lower crust lies at $T \geq 800^\circ\text{C}$, and isotherms are inverted beneath the plateau by the combination of outward flow of the channel and inward flow of cool pro-mantle lithosphere. Surface denudation has exhumed a narrow, roughly symmetrical region of middle crust at the erosion front; near-surface isotherms in this region are strongly perturbed as a result of rapid exhumation. This stage (33 My=21 Ma) corresponds approximately to the time of widespread anatexis, leucogranite intrusion, and high-temperature 'Neohimalayan' (M2) metamorphism in the GHS. Both the MCT and the STD were active at this time [e.g., *Hodges et al.*, 1992].

By ca. 39 My, focused surface denudation at the plateau flank has thinned and weakened the upper crust, allowing it to flow outward with the underlying channel [*Beaumont et al.*, 2004]. This leads to a change in tectonic style at the erosion front from a symmetrical structure (Fig. 2b) to an asymmetrical, overthrust structure (Fig. 2c,d). A more detailed discussion of the flow modes and tectonic styles resulting from interactions between the channel and overlying and underlying crustal layers is presented in *Beaumont et al.* [2004]. By 42 My (12 Ma) the channel has reached the plateau flank and is being actively extruded (Fig. 2c); the exhumed channel is substantially thinner than its equivalent at depth. This time corresponds approximately to the onset of observed metamorphism in the LHS [e.g., *Harrison et al.*, 1997; *Catlos et al.*, 2001; *Vannay et al.*, 2004], and with later stages of movement on both the MCT and STD [*Copeland et al.*, 1991; *Edwards and Harrison*, 1997; *Harrison et al.*, 1997].

Figure 2d shows the configuration of deformed crust and isotherms at the end of the model (54 My), corresponding to the present day. As discussed by *Beaumont et al.* [2004], the model crustal thickness, geometry at the erosion front, and position of the model 'suture' are consistent with observations from the Himalayan-Tibetan system. Surface erosion and channel flow have produced a significant loss of crustal section across the "MCT" (Fig. 2d; between vertical

markers -2 and -10). Temperatures of 800-950°C beneath the model plateau (Fig. 2d) are compatible with the inferred presence of partial melt beneath the Tibetan plateau [e.g., *Nelson et al.*, 1996], and with P - T conditions recorded by Tertiary granulite xenoliths in volcanic rocks from Tibet [*Hacker et al.*, 2000] and the Pamirs [*Ducea et al.*, 2003]. On the pro-side of the model, high mid-crustal temperatures do not correspond to anomalously hot sub-orogenic mantle (Fig. 2d), because cool pro-mantle lithosphere is rapidly and continuously advected beneath the plateau. The system is therefore characterized by a high thermal Peclet number and does not reach conductive equilibrium at any stage after the onset of convergence.

3.2. Crustal-scale metamorphism

The thermal evolution of the model mainly reflects the distribution of thickened radioactive upper crust (Fig. 2) and advection of isotherms by the combined effects of channel flow and surface denudation. By 42 My, $T > 900^\circ\text{C}$ in the lower crust beneath the central plateau, and the 800°C isotherm extends through the middle crust to the plateau edge (Fig. 2c,d). The effects of these high middle- to lower crustal temperatures on the metamorphic evolution of the model orogen are shown in simplified 'facies' diagrams (Fig. 3). These are constructed by comparing the distribution of T_{max} and $P@T_{max}$ within the model to a simplified metamorphic grid (inset, Fig. 3), assuming that peak metamorphic assemblages mainly reflect these conditions.

At 21 My, before the onset of erosion and exhumation, metamorphic facies boundaries follow corresponding isotherms. Most of the orogenic crust lies within the greenschist and amphibolite facies, with migmatite restricted to the orogenic core. At this time the lowermost crust lies in the eclogite facies. However, this early eclogite is overprinted by granulite during subsequent model evolution (see section 9). During the early stages of erosional exhumation (33 My), when amphibolite begins to reach the surface, isotherms are strongly perturbed beneath the erosion front but still mainly correspond to facies boundaries because the orogen is still heating

up. By 42 My, isotherms cross metamorphic facies boundaries beneath the erosion front, where high-grade rocks are brought to the surface by efficient exhumation. In the final 10 My of model evolution, declining erosion rates and consequent relaxation of isotherms lead to significant differences between isotherms and facies boundaries at the orogenic front. At this stage, the 700°C isotherm that marks the limit of the melt-weakened zone, and hence the tip of the 'active' channel, lies beneath the plateau flank; migmatite extruded at the erosion front at the end of the model therefore represents 'fossil' channel material. As discussed further below (section 6), the juxtaposition of outward-flowing high-grade channel material with incoming lower-grade material (tracked points in Fig. 3) contributes to the 'inverted' metamorphic sequence in the vicinity of the erosion front.

By 33 My, a dome-like region of migmatite-grade rocks is present on the retro-side of the model suture. This is inherited from early crustal thickening and heating in the orogenic core, and subsequent crustal thinning and minor exhumation in this region associated with the formation of the plateau. Other models in this series [Beaumont *et al.*, 2001a, 2003, 2004] produce domes between the erosion front and the suture in response to underthrusting of strong lower crust and variations in upper crustal strength and surface denudation rate. Some of these model features may be analogous to the north Himalayan gneiss domes.

4. Metamorphic evolution of selected "GHS" points

A complete record of pressure (P), temperature (T), depth (z), and horizontal position (x) with time (t) is calculated for pre-defined points. These results are presented below as particle (x - z), P - T , T - t , and z - t paths for four "GHS" (Fig. 4) and four "LHS" points (Fig. 6). Although the eight points follow different trajectories through the model, all are exhumed at approximately 54 My in the vicinity of the orogenic front, and thus illustrate the contrasting metamorphic histories

that might be encountered on a 'transect' across the model orogen. The metamorphic histories of the tracked points are first described separately; the resulting pattern of metamorphism near the orogenic front is discussed later (section 6, Fig.8).

4.1. Particle paths

Particle (x - z) paths for the four selected "GHS" points (G1-G4) are presented in Figure 4a. All four points reverse their transport direction, relative to incoming pro-crust, during the model evolution so that their final positions are pro-ward of their initial positions. Points G1 and G2 are entrained within the hot channel ($T_{max} > 700^{\circ}\text{C}$; Fig. 4b), whereas points G3 and G4 lie at higher structural levels in crust that flows outwards with the underlying channel. The points, which initially lie 300-400 km pro-ward of the model suture, are incorporated into the growing orogen within 12 My of the onset of collision. All reach their maximum burial depths and maximum retro-ward positions by 18-24 My, when they become entrained in, or carried above, the low-viscosity channel. From ca. 24-42 My they are translated back towards the pro-side of the system at gradually shallowing depth. All four points are exhumed rapidly in the vicinity of the erosion front during the last ca. 6 My of model evolution. The initially deepest and most retro-ward ('north') point (G1) emerges immediately above the model MCT (i.e., furthest 'south'). Points G2-G4, originally aligned in a vertical column 70 km pro-ward ('south') of G1, emerge in their original stratigraphic order, with the initially shallowest point structurally highest above the "MCT" and therefore also the furthest 'north' at the surface. The total lateral separation among the four points at the end of the model is ca. 30 km. The lateral distance between points G1 and G2, which are entrained in the hot channel, decreases from 70 km to ca. 10 km, consistent with thrust-sense displacement. In contrast, the lateral separation between G2, G3, and G4 increases, consistent with normal-sense displacement. In nature, the reversal in transport direction and lateral flow in the hot channel, combined with small-scale (< 5 km) rheological heterogeneities,

would produce locally complex flow regimes and structures. Large-scale variations in lower crustal strength can produce significant structural complexity in the models [e.g., HT-HET, Fig. 14 of *Beaumont et al.*, 2004]. However, for the crustal properties assumed here, velocity profiles (Fig. 2), orientations of originally horizontal marker layers above the "MCT", and smooth, nearly parallel particle paths (Fig. 4a) show that channel flow does not lead to overturning or mixing on the scale of the crust.

4.2. *P-T* evolution

P-T paths from the four selected "GHS" points all form broad loops with three distinct stages (Fig. 4b). The first stage involves burial and heating along relatively steep dP/dT prograde paths in the kyanite field until the onset of channel flow at 18-24 My. For points G2-G4, the second *P-T* stage involves an interval of nearly isobaric heating corresponding to pro-ward translation with the channel. Heating at nearly constant depth results from the combined effects of outward heat advection by the channel and radioactive heat production within the thickened crust. Most points cross from the kyanite to sillimanite field toward the end of this stage; points G1 and G2 cross into the muscovite dehydration melting field at ca. 33 My and ca. 36 My respectively. Point G1 shows a significant interval of near-isothermal decompression between ca. 30 and 40 My (Fig. 4b), representing about 20 km of vertical transport over a lateral distance of ca. 250 km in the channel (Fig. 4a). Although it remains at depth beneath the plateau, G1 does not heat up significantly during this stage because this level of the channel is already close to its maximum temperature (Fig. 3). In all cases, the third *P-T* stage is characterized by cooling and decompression along moderate dP/dT retrograde paths that lie mainly in the sillimanite field (Fig. 4b), with some points passing through the andalusite field in the final stages of exhumation (see also Fig. 5).

4.3. Burial, heating, exhumation, and cooling

Figure 4c presents depth-time ($z-t$) and temperature-time ($T-t$) paths for the same points. In all cases, exhumation begins shortly after the "GHS" points are first entrained by the channel (18-24 My), but significant cooling does not occur until ca. 10-20 My later, when the channel reaches the plateau flank. The delayed cooling reflects the combined effects of lateral heat advection and internal heating by radioactive decay within the thickened crust. Rapid cooling (75-100°C/My) accompanies rapid exhumation (2-3 km/My) during the last 10 My of model evolution.

4.4. Comparison of model results with $P-T-t$ data from the GHS

An important test of model HT1 is provided by comparing predicted $P-T$ and $T-t$ paths with $P-T-t$ data from the orogen. Because closely spaced points at the surface may have followed quite different $P-T$ trajectories (Fig 4), model $P-T$ paths must be compared with 'single-point' $P-T$ and $T-t$ data from real rocks. Unfortunately, it is difficult to extract reliable $P-T$ paths from single GHS samples because protracted high temperatures have largely obliterated the prograde mineral assemblages and/or garnet growth zoning that might have recorded the early part of the metamorphic history [e.g., Davidson *et al.*, 1997; Vannay and Grasemann, 1998; Fraser *et al.*, 2000]. For similar reasons, it is not possible to obtain $T-t$ data for the early history of the GHS. Figure 5 presents model $P-T$ and $T-t$ paths from the three highest-grade "GHS" points compared with data from the GHS of the central and western Himalaya.

Steep to moderate prograde $P-T$ trajectories recorded by zoned garnets from the GHS in the western Himalaya [Vance and Mahar, 1998; Walker *et al.*, 2001] lie within the range of prograde path segments predicted by model "GHS" points (G1, G2; Fig. 5a). The model also provides an explanation for the nearly isobaric heating paths reported by some authors [e.g., Swapp and Hollister, 1991; Vannay and Grasemann, 1998; Rolland *et al.*, 2001] in terms of heating during

lateral transport in the outward-flowing channel (G2, G3; Fig. 5a). Isothermal decompression paths reported from southern Tibet [e.g., *Hodges et al.*, 1993] lie within the range of model "GHS" paths, although at lower P - T conditions than the isothermal decompression path segment for point G1 (Fig. 5a). Model predictions are also compatible with fluid inclusion data [*Craw*, 1990] interpreted to record a segment of the retrograde history of the GHS in central Nepal.

In Figure 5b, intrusion and cooling ages of two high Himalayan leucogranites [*Searle et al.*, 1997, 1999a] and peak metamorphic and cooling ages from single and/or closely spaced samples in the GHS of central Nepal [*Copeland et al.* 1991; *Catlos et al.*, 2001] are compared with representative model T - t paths. The leucogranite data indicate rapid cooling at rates comparable to those predicted by the model (75-85°C/My), but 15-20 My earlier. There are two possible explanations for this discrepancy. Either the erosion model needs adjustment to allow for earlier rapid exhumation followed by slower cooling in the last 15 My of the model, or the leucogranite T - t data reflect post-intrusion cooling to ambient low temperatures and are not representative of the GHS as a whole. Given their high structural position in the upper GHS, we infer that rapid cooling of the leucogranites reflects intrusion into cool country rocks and/or cooling associated with normal faulting and possible fluid flow within the STD zone [e.g., *Guillot et al.*, 1995]. Model T - t paths agree well with times of peak metamorphism from the GHS of central Nepal [*Coleman*, 1998; *Catlos et al.*, 2001]. However, observed mica cooling ages [*Copeland et al.*, 1991; *Catlos et al.*, 2001] are ca. 5-10 My older than predicted by the model (Fig. 5b; section 7).

5. Metamorphic evolution of selected "LHS" points

5.1. Particle paths

Figure 6a shows particle paths for four "LHS" points (L1-L4) that are exhumed together near the orogenic front at ca. 54 My. All four points initially lie 1300-1700 km pro-ward of the

model suture. They are transported into the orogen after 36-42 My of convergence, reaching their maximum burial depths and retro-ward positions in the last 6-12 My of model evolution. They are then rapidly exhumed and transported pro-ward in the footwall of the overlying channel as the orogen advances toward its foreland. At the end of the model, all four "LHS" points lie structurally below the "MCT", significantly retro-ward of their initial positions. "LHS" points originating at deeper crustal levels closer to the model suture are incorporated earlier, buried more deeply, reach higher temperature, and emerge closer to the "MCT" than shallower points that enter the model orogen later. In contrast to "GHS" points, their relative stratigraphic positions are reversed, with the exception of points L3 and L4. In this case, L4 enters the orogen earlier and at a shallower level than L3, but is caught up beneath the advancing channel and eventually exhumed immediately below the model "MCT". In model HT1, originally horizontal layers in the footwall of the "MCT" are shortened, steepened, and eventually overturned beneath the advancing channel (Fig. 2). In nature, imbrication along discrete thrust faults, which are not possible in the present continuum model, could achieve a similar amount of shortening without overturning the strata [e.g., *Robinson et al.*, 2003].

5.2. *P-T* evolution

Points L1 and L2 form tight 'hairpin' *P-T* loops (Fig. 6b), in which *T_{max}* and *P_{max}* are reached at about the same time, reflecting short residence times within the model orogen. Both L3 and L4 cross into the sillimanite field during exhumation, and they are also the only "LHS" points to approach the melting field. In these cases, some heating during decompression is attributable to their earlier and deeper burial and longer residence time in the model orogen relative to L1 and L2. The *P-T* path for L4 shows small fluctuations in *P* and *T* associated with its proximity to the overlying channel (Fig. 6a, 6b). Although these fluctuations could be artifacts

of the model, complexly zoned garnet from immediately below the MCT in central Nepal [Kohn *et al.*, 2001] may record a similarly complicated P - T history.

5.3. Burial, heating, exhumation, and cooling

The T - t histories of all four "LHS" points display rapid heating to T_{max} within 5-10 My of initial burial (Fig. 6c), as they are carried into the high-temperature region beneath the advancing channel. In contrast to the "GHS", P_{max} in the "LHS" is reached at 40-50 My rather than at 20-30 My, and the onset of cooling coincides approximately with the onset of exhumation. Rapid cooling in the last 5-8 My of model evolution accompanies rapid exhumation by thrusting and erosion as the model orogen propagates towards its foreland. Cooling rates in the last 5-10 My of the model are typically 60-80°C/My, at exhumation rates of 2-3 km/My.

5.4. Comparison of model results with P - T - t data from the LHS

Figure 7 presents representative model P - T and T - t paths from the "LHS" compared with data from the LHS of the central Himalaya. LHS rocks have a much shorter metamorphic history, and correspondingly better potential to record prograde paths, than GHS rocks. P - T paths from zoned garnets from the lower MCT zone in central Nepal [Kohn *et al.*, 2001] overlap with model "LHS" P - T paths. However, paths recorded at higher structural levels reach higher P at lower T than any of the tracked model points (Fig. 7a). The structural duplication reported from the MCT zone in this region [Catlos *et al.*, 2001] suggests that the discrepancy may be related to the presence of a younger structure that exhumed LHS rocks from deeper levels than predicted by the present continuum model. T - t data from closely spaced LHS samples [Copeland *et al.*, 1991; Catlos *et al.*, 2001] agree well with predicted model T - t paths, although somewhat earlier heating is suggested by some LHS data (Fig. 7b).

6. Peak grade profiles

The model tracks T_{max} , $P@T_{max}$, and the times at which T_{max} and P_{max} were reached ($t@T_{max}$, $t@P_{max}$) for points at the model surface in any specified region at any specified time. These peak grade and age profiles are particularly useful for comparing model predictions with thermobarometric and geochronological data from transects across orogens [e.g., *Jamieson et al.*, 1996]. In model HT1, peak temperatures rise steeply through the "MCT" zone, across the "MCT", and into the lower "GHS", where they decline gradually (Fig. 8a). Metamorphic pressures also increase sharply and decline abruptly, peaking just above the "MCT" (Fig. 8b). The resulting 'inverted' metamorphic pattern, which is characteristic of crustal-scale ductile thrust zones [e.g., *Jain and Manickavasagam*, 1993; *Jamieson et al.*, 1996; *Grujic et al.*, 1996], is accentuated in this case by juxtaposition at the surface of the outgoing "GHS" with the incoming "LHS".

There is good agreement between model peak grade profiles (Fig. 8a,b) and metamorphic T - P data from the Langtang region of central Nepal [*Inger and Harris*, 1992; *Macfarlane*, 1995; *Fraser et al.*, 2000]. In both nature and the model, the width of the peak grade profile is sensitive to the interplay of structure, topography, and denudation [e.g., *Grujic et al.*, 2002; *Duncan et al.*, 2003]. A combination of these factors could produce observed peak grade profiles that are discontinuous [e.g., *Kohn et al.*, 2001], duplicated, narrow, or broad [e.g., *Searle et al.*, 2003; *Vannay et al.*, 2004] relative to those predicted by model HT1.

The model "MCT" corresponds to the protolith boundary between incoming material and the outward-flowing channel, and lies within a zone of high strain encompassing both the upper "LHS" and the extruded channel (Fig. 2d, 8d). In parts of the Himalaya, the MCT is a mappable protolith boundary [e.g., *Grujic et al.*, 1996; *Davidson et al.*, 1997]. However, in many places the inferred position of the MCT lies within a zone of highly strained gneisses lacking clear

lithologic markers, leading to differences in the way the MCT is defined in different regions [e.g., *Hubbard, 1989; Kohn et al., 2001; Searle et al., 2003; Robinson et al., 2003*]. The problem is compounded by the presence of multiple thrust-sense structures within the MCT zone in some places [e.g., *Hodges et al., 1996; Catlos et al., 2001; Vannay et al., 2004*]. In comparing model results with data, we have used the position of the MCT as defined in the source papers.

The position of the model "STD" is more difficult to define. The top of the low-viscosity channel ($T_{max} > 700^{\circ}\text{C}$) is a zone of high normal-sense shear strain that lies 10-12 km above the "MCT" ("STD", Fig. 8). The high strain zone is overlain by a broad region of middle and upper crust that has flowed outward with the channel. This region of the model displays distributed normal-sense shear and passes gradually upward into lower grade ($T_{max} < 350^{\circ}\text{C}$) and less deformed rocks of the weak upper crust ("TS"; Fig. 8a,d), analogous to the Tethyan series (TS). Particle paths for points within this zone, like those between the "MCT" and "STD", show a reversal in transport direction (G3, G4; Fig. 4) and their surface positions are consistent with normal displacement relative to the top of the channel. In nature, the STD is recognized as a normal fault, fault system, or ductile shear zone that separates metamorphic rocks of the GHS from lower grade rocks of the TS [e.g., *Burg et al., 1984; Burchfiel et al., 1992; Searle and Godin, 2003*]. In many places, multiple normal faults and shear zones have been documented [*Coleman, 1996; Searle et al., 2003; Searle and Godin, 2003*], and in some cases the rocks lying between them have been mapped as separate units [e.g., Everest series, *Searle et al., 2003*; Chekha Formation, *Grujic et al., 2002*]. Since model HT1 is a continuum mechanics model that does not predict discrete faults, structures corresponding to the observed STD could lie anywhere between the normal-sense shear zone at the top of the extruded channel ("STD") and the top of the exhumed middle crust (Fig. 8d). The region between the model "STD" and "TS" could

correspond to the upper GHS, the lower TS, or an intervening unit. For purposes of discussion, all of the material between the model "MCT" and the top of the exhumed middle crust is included here with the model "GHS".

Although the initial positions of the eight tracked points are separated by up to 1400 km laterally and more than 10 km vertically, by the end of the model they lie within 40 km of each other at the model surface (Fig. 8d). The loss of section across the "MCT", estimated by comparing the initial positions of "LHS" point L3 and "GHS" point G1, is about 950 km; the loss of section across the orogenic front, between the lowermost "LHS" and uppermost "GHS", is about 600 km [Beaumont *et al.*, 2004]. These distances lie within the range of those estimated from geological data [e.g., Johnson, 2002]. All of the material exhumed at the model orogenic front is derived from the pro-side of the system (equivalent to India) and the model is thus compatible with tectonic reconstructions involving a continuous Indian margin [e.g., Myrow *et al.*, 2003]. The extreme condensation of the model section results from the combination of variable flow velocities in the high-strain region within and below the channel, the reversal in flow direction associated with channel flow, and focused surface denudation that removes a large volume of upper and middle crust from the central part of the model.

Agreement between model and observed peak grade profiles is a necessary, but not sufficient, test of the model. Equally good correspondence, within the error of the data and the spatial resolution of the model, can be achieved by a number of different model styles and at more than one time during the evolution of a given model. For example, the peak grade profiles from model HT1 at 51 My also fit the *P-T* data reasonably well, and other models with different convergence rates and/or different surface denudation functions produce peak grade profiles that match the *P-T* data within error [e.g., Model 3, Beaumont *et al.*, 2001a]. It is therefore necessary to test model predictions against other constraints, particularly geochronological data.

7. Times of peak metamorphism and cooling

The times at which points at the model surface at any given time reached their peak temperature ($t@T_{max}$), or cooled through specified temperatures, can be plotted as age profiles across the model surface (Fig. 8c). Values of $t@T_{max}$ rise steeply from <12 Ma in the "LHS" to >15 Ma across the "MCT", leveling out at about 20 Ma in much of the "GHS". This pattern reflects the juxtaposition of "GHS" points, which have a prolonged residence time within the model orogen, with recently accreted "LHS" points. Within the "GHS", $t@T_{max}$ declines slightly across the exhumed channel, because material near the channel base is incorporated into the orogen somewhat earlier and therefore reaches T_{max} slightly before material near the channel top (Fig. 4). This pattern is reversed at higher structural levels, where T_{max} is lower. These results are broadly compatible with monazite data from the LHS and GHS in the Marsyandi region of west-central Nepal [Catlos *et al.*, 2001], although the observed GHS ages are somewhat older than the model predictions (Fig. 8c). At distances greater than about 15 km below the "MCT" and greater than about 35 km above it, where $T_{max} < 350^{\circ}\text{C}$, model cooling ages do not reflect the tectonics ('ages not reset'; Fig. 8c). In nature, pre-Himalayan or disturbed isotopic ages would be expected in these regions [e.g., Catlos *et al.*, 2001].

The predicted times of cooling through 700°C (t_{700}), 500°C (t_{500}), and 350°C (t_{350}), corresponding roughly to the closure temperatures of monazite, hornblende, and muscovite respectively, show little spatial variation across the model surface (Fig. 8c). Above the "MCT", all t_{700} points lie between 10 and 7.5 Ma, t_{500} points lie between 7.5 and 4 Ma, and t_{350} points lie mainly between 7.5 and 2 Ma, with most < 4 Ma. As evident from the similarity of $t@T_{max}$ and t_{350} ages near the top of the "GHS", where T_{max} is close to 350°C (Fig. 8a, 8c), some t_{350} values approximate growth rather than cooling ages. In the "LHS", where $T_{max} < 700^{\circ}\text{C}$, model

results for t_{500} and t_{350} points are very similar to those from the "GHS". The predicted t_{350} ages in the "LHS" agree well with muscovite ages from the LHS in the Marsyandi section [Fig. 8c; *Catlos et al.*, 2001], but above the "MCT" model t_{350} ages are generally younger than observed GHS muscovite ages (Fig. 8c, 9).

In Figure 9, reported ages from the Himalaya of Nepal are compared with times of peak metamorphism and cooling for points at the surface at the end of the model. Monazite and zircon U-Pb ages from leucogranites intruded into the GHS fall in the range 16-24 Ma. This also corresponds to the time of the pervasive high-temperature, medium- to low-pressure Neohimalayan (M2) metamorphism associated with widespread anatexis in the GHS [e.g., *Vannay and Hodges*, 1996; *Coleman*, 1998; *Catlos et al.*, 2001; *Searle et al.*, 2003]. Model results for $t@T_{max}$ in the "GHS" (Fig. 8c, 9b) fall in the range 12-22 Ma, in good agreement with the observed times of leucogranite intrusion and M2 metamorphism. An earlier, relatively higher-pressure Barrovian metamorphism in the GHS, generally referred to as Eohimalayan (M1), has been dated at ca. 28-36 Ma in a few localities [e.g., *Hodges et al.*, 1996; *Vance and Harris*, 1999; *Simpson et al.* 2000]. This corresponds well to model times of maximum burial ($t@P_{max}$ = 26-36 Ma; Fig. 9b), which record when material transported into the orogen at an early stage becomes entrained in the channel flow zone (Fig. 4a). In nature, a significant change in structural and metamorphic style would be expected to coincide with the reversal in transport direction and the corresponding change from progressive burial to lateral return flow.

Monazite U-Pb ages from the LHS [*Harrison et al.*, 1997; *Catlos et al.*, 2001] form a relatively tight cluster at 4-12 Ma (Fig. 9a), corresponding well with both $t@T_{max}$ and $t@P_{max}$ for the "LHS" (Fig. 9b). In the model, the young ages come from material recently transported into the orogen from the pro-side of the system. This material is first buried beneath the advancing flank of the orogen and then transported back to the surface beneath the channel (Fig.

6a, 8d) as deformation in the model orogen propagates towards its foreland. In the model, the age difference between the "LHS" and "GHS" does not correspond to a change in the tectonic boundary conditions, but reflects surface juxtaposition of points transported into a continuously evolving system at different times. Muscovite $^{40}\text{Ar}/^{39}\text{Ar}$ ages from the GHS and associated leucogranites in Nepal fall mainly in the range 12-20 Ma (Fig. 9a), with detrital muscovites from catchment basins draining the GHS falling in the same range [Brewer *et al.*, 2003]. At its younger end, the observed GHS age range overlaps with the generally younger muscovite ages from the LHS. Model t_{350} ages form two distinct populations, one at <8 Ma (both "LHS" and "GHS" results) and one at 16-20 Ma ("GHS" only). Although the model and observed age ranges overlap, most model "GHS" t_{350} ages are younger than muscovite ages from the GHS.

The discrepancy between model t_{350} results and observed muscovite ages suggests that "GHS" denudation rates (and therefore cooling and exhumation rates) have been overestimated. As discussed by *Beaumont et al.* [2004], model HT1 is probably a denudational end member. In particular, strain localization, which is not included in the model, would focus deformation on specific structures at the orogenic front (e.g., "MCT", "STD"), leading to efficient channel extrusion at lower overall denudation rates as well as more realistic model geometries in this region. Alternatively, high model cooling rates (Fig. 4c, 6c) may correspond to higher closure temperatures than the nominal value of 350°C used to compare observed muscovite $^{40}\text{Ar}/^{39}\text{Ar}$ ages with model T-t paths. For example, a closure temperature of $450 \pm 50^\circ\text{C}$ has recently been calculated for some Sutlej Valley muscovites [Vannay *et al.*, 2004]. In the present case, a closure temperature $>500^\circ\text{C}$ would be required to produce significantly better agreement between the model and the data (Fig. 5b). Although we have chosen not to refine the current model (see section 10.4), improving the agreement between predicted and observed cooling ages is a high priority for future investigations.

8. Erosion record

Detrital mineral suites and cooling age vs. depositional age studies in sedimentary basins are widely used to constrain denudation and exhumation histories of the Himalaya and other orogenic belts [e.g., *DeCelles et al.*, 1998; *Najman and Garzanti*, 2000; *White et al.*, 2002; *Najman et al.*, 2002]. In addition to tracking the position of the erosion front and denudation rate in model HT1 (Fig. 2), we also record the peak metamorphic grade of points exposed at, and then eroded from, the model surface at different times (Fig. 10). This can be used as a general guide to the sequence and times of first appearance of metamorphic minerals in foreland basin sediments, assuming that the material is deposited soon after erosion.

In model HT1, erosion begins at 30 Ma (Fig. 10a), and high erosion rates are maintained from ca. 24-14 Ma, peaking at ca. 17 Ma. After ca. 15 Ma, erosion rate declines gradually as model surface slopes adjust to changes in the erosion function. Initially, the eroded points consist entirely of very low-grade material ("sub-greenschist"; Fig. 10b). "Greenschist" first appears just before 25 Ma and from ca. 24-18 Ma is the dominant material being eroded. "Amphibolite" first appears at ca. 22 Ma and is most abundant at ca. 15 Ma; "migmatite" first appears at ca. 15 Ma (Fig. 10b), near the end of the high erosion rate interval. The peak grade conditions of eroded amphibolite and migmatite points lie in the sillimanite field, although the corresponding P - T paths all pass through the kyanite field before reaching T_{max} . As erosion rates decline toward the end of the model, sub-greenschist material once again dominates the eroded assemblage.

Studies of detrital minerals in foreland basin deposits in northern India [*White et al.*, 2002; *Najman et al.*, 2002] indicate that garnet first appears at about 22 Ma, staurolite at about 20 Ma, and kyanite by about 13 Ma. Kyanite and/or sillimanite are present after about 11 Ma in sediments from western Nepal [*DeCelles et al.*, 1998]. In nature, garnet normally first appears in

greenschist facies metasediments; the model suggests that it should appear in detritus sometime after 25 Ma (Fig. 10b). Staurolite, which is characteristic of amphibolite facies metasediments, should appear at about 20 Ma. Kyanite and/or sillimanite could be present in either amphibolite or migmatite, but typically first appear at somewhat higher grade than the first appearance of staurolite. The model predicts that they should appear at the surface sometime after 20 Ma, and should become relatively more common in younger sediments, with sillimanite probably appearing after kyanite. Although limitations in both the model and the data preclude a more detailed comparison at this time, we conclude that the erosion model is generally consistent with observed detrital mineral assemblages.

9. Lower crustal metamorphism

Although this paper focuses on the mid-crustal metamorphism characteristic of the present-day Himalaya, the thermal and mechanical evolution of the lower model crust may shed light on the significance of some Himalayan eclogites [e.g., *Lombardo and Rolfo, 2000*], and may also be relevant to the interpretation of high-grade metamorphism in large, deeply eroded orogens. Figure 11 illustrates particle paths and P - T - t paths for two points (E1, E2) buried at depths of ca. 40 km at the end of the model, and which would therefore lie close to the surface if post-orogenic denudation restored the crust to its normal thickness.

Point E1, initially located 400 km from the model suture, exhibits continuous burial along a steep prograde path, followed by an abrupt transition to decompression when it is entrained near the base of the model channel (ca. 24 My). This point spends ca. 15 My at eclogite-facies conditions ($P > 16$ kb; Fig. 11a), and for the last 20 My of the model lies at nearly constant, granulite-facies conditions (ca. 850°C, 10.4 kb). Point E2, initially located 800 km from the model suture, also follows a steep prograde path, although its burial history is more complex (24-

36 My). High-pressure conditions are maintained for over 20 My (Fig. 11), followed by near-isothermal decompression to granulite-facies conditions by the end of the model (ca. 925°C, 11.4 kb). In both cases, prolonged residence time at high temperature should lead to extensive overprinting of early eclogite by granulite. High-pressure metamorphism is diachronous because material is fed continuously into the lower model crust (Fig. 11b); there is no single eclogite-facies 'event'. In the later stages of model evolution, the 800°C isotherm lies at mid-crustal levels, nearly parallel to the plateau surface (Fig. 3). Granulites formed in this setting should be laterally extensive, and dominated by subhorizontal structures associated with channel flow (Fig. 2, 3) and/or post-orogenic ductile thinning [e.g., *Jamieson et al.*, 2002]. A comparison between the full dynamic pressure (P_{dyn}), including the effect of burial and tectonic stress, and lithostatic pressure (P_{lith}) resulting from burial depth alone (Fig. 11c), indicates that 'tectonic overpressure' [e.g., *Mancktelow*, 1995] is not significant in the low-viscosity model channel.

Model P - T - t paths for tracked points G1-G4 do not cross into the eclogite field (Fig. 4, 6), and points E1 and E2 still lie a considerable distance from the orogenic front at the end of the model. This suggests that Himalayan eclogite now at the surface probably originated deeper in the crust and somewhat closer to the suture than any of the tracked model points, and should therefore have pre-M1 ($t@P_{max}$) ages. In models where the strength of the lower crust varies laterally [e.g., HT-HET; Fig. 14c of *Beaumont et al.*, 2004], lower crustal material can be detached from its substrate and entrained by the channel flow, eventually reaching the surface as isolated fragments near the base of the exhumed channel.

Eclogite with early Himalayan ages [e.g., *de Sigoyer et al.*, 2000] has been reported from a few localities in both the western [*Pognante and Spencer*, 1991] and east-central Himalaya [e.g., *Lombardo and Rolfo*, 2000]. The contrast between the well preserved western Himalayan eclogites, which locally contain coesite [e.g., *O'Brien et al.*, 2001; *Treloar et al.*, 2003], and

those further to the east, which are strongly overprinted by granulite, has been attributed to contrasting exhumation histories [e.g., *Lombardo and Rolfo*, 2000]. Model HT1 offers no insight into the formation or initial exhumation of coesite-bearing eclogites in the Himalaya or elsewhere because the lower model crust does not reach ultra-high pressure conditions and there is no mechanism for returning subducted material to crustal levels. However, entrainment of eclogitic lower crust in the channel could account for the strongly overprinted eclogite bodies near the base of the GHS in the Everest region [e.g., *Lomabrdo and Rolfo*, 2000], or in deeply eroded granulite or migmatite terranes elsewhere [e.g., *Ketchum and Davidson*, 2000].

10. Discussion

10.1. Inverted metamorphism

The inverted metamorphism associated with the MCT zone has been variously attributed to heat transfer from a hot upper crustal plate [e.g., *LeFort*, 1975; *Swapp and Hollister*, 1991; *Royden*, 1993; Fig. 12a], frictional heating along the MCT [e.g., *Molnar and England*, 1990; *England and Molnar*, 1993; *Harrison et al.*, 1998; Fig. 12b], underplating by accreted radioactive material [e.g., *Huerta et al.*, 1999], deformation of pre-existing isograds [e.g., *Searle and Rex*, 1989; *Hubbard*, 1996; Fig. 12c], and syn-metamorphic ductile shear [e.g., *Brunel and Kienast*, 1986; *Jain and Manickavasagam*, 1993, *Jamieson et al.*, 1996] that in some models has been linked to extrusion of a crustal wedge [e.g., *Hodges et al.*, 1993, 1996; *Grujic et al.*, 1996; *Vannay and Grasemann*, 2001; Fig. 12d]. Some of these interpretations focus only on the MCT [e.g., *Molnar and England*, 1990; *Royden*, 1993], while others also account for coeval thrusting on the MCT and extension on the STD [e.g., *Searle and Rex*, 1989; *Grujic et al.*, 1996].

In model HT1, inverted metamorphism results from a combination of syn-metamorphic ductile shear and outward flow of the hot mid-crustal channel. Asymmetric, inverted peak grade

profiles are characteristic of models in which material points are exhumed within and adjacent to crustal-scale, thrust-sense shear zones in response to focused surface denudation [e.g., *Jamieson et al.*, 1996; *Grujic et al.*, 1996]. The variable velocity gradient across the shear zone leads to differential exhumation and juxtaposition of material points that originated at different crustal levels (e.g., Fig. 8d). Inversion of a sequence by distributed ductile shear can be either syn-metamorphic or post-metamorphic [e.g., *Hubbard*, 1996]; in the present case it is clearly syn-metamorphic, because material continues to heat up until the final stages of exhumation (Fig. 3). Although inverted metamorphic sequences do not require inverted crustal isotherms [e.g., *Jamieson et al.*, 1996], in model HT1 the extruded channel acts like a hot upper plate [e.g., *Royden*, 1993], and crustal isotherms are inverted beneath the plateau flank (e.g., Fig. 2, 3). There is no simple correspondence between these isotherms, which evolve with time (Fig. 3), and the inverted peak grade profile, which is defined by material points that reached T_{max} at different times and in different places in the model crust (Fig. 4a, 6a). The observed T_{max} profile therefore does not represent a thermal gradient, and present-day isograds need not represent past isotherms.

In both nature and model HT1, metamorphic temperatures and pressures peak in the lower part of the GHS and then decline, defining a 'normal' metamorphic sequence in the upper GHS. This has been interpreted as an exhumed crustal section [e.g., *Macfarlane*, 1995]; however, in model HT1 the points defining this pattern did not represent a vertical section prior to exhumation (e.g., Fig. 8d, 6 Ma point positions). Others have concluded that there is very little difference in peak pressure across the GHS [e.g., *Vannay and Grasemann*, 1998, 2001] and have used this observation to constrain tectonic models for ductile extrusion. Channel flow models that evolve more complex exhumation styles in the vicinity of the orogenic front, for example by expelling domes [*Beaumont et al.*, 2003, 2004], can produce broader peak grade profiles at lower

and/or higher structural levels, depending on the details of model evolution. This may account for the differences between the "GHS" profile produced by model HT1 and the broad regions of nearly constant, relatively low pressure reported from some GHS sections [e.g., *Vannay and Grasemann, 1998; Searle et al., 2003*]. Alternatively, late-stage leucogranite intrusion, extension in the upper crust above the channel [e.g., *Beaumont et al., 2001a, 2004*], or protracted transport in the hot channel at gradually declining depth could induce partial re-equilibration of peak metamorphic assemblages at $P < P@T_{max}$.

In some models, the driving force for ductile extrusion is the pressure gradient imposed by narrowing of a crustal wedge at depth [*Grujic et al., 1996; Vannay and Grasemann, 2001; Fig. 12d*]. In model HT1, extrusion is driven by the differential pressure between the plateau and the foreland [e.g., *Clark and Royden, 2000; Hodges et al., 2001; Beaumont et al., 2001a, 2004*], and does not require the channel to narrow. Although seismic data [*Nelson et al., 1996; Hauck et al., 1998; Haines et al., 2003*] indicate a wedge-shaped geometry beneath the orogenic front, the present-day geometry may have developed after Miocene extrusion of the channel [e.g., *Beaumont et al., 2001a, 2004; Grujic et al., 2002*].

10.2. *P-T-t* paths and tectonic style

The range of *P-T-t* path styles observed from the Himalaya [e.g., *Guillot et al., 1999*] has been attributed to a range of tectonic processes including one or more discrete phases of thrusting, post-thrusting thermal relaxation, and exhumation associated with either syn-orogenic erosion or extensional denudation. For example, *Vannay and Grasemann [1998]* attributed isobaric heating paths in the GHS to thermal relaxation at constant depth following the end of underthrusting. Isothermal decompression paths from a number of GHS locations [e.g., *Hodges et al., 1993; Davidson et al., 1997; Daniel et al., 2003*] have been linked to normal faulting on the STD, rapid erosion above the MCT, or a combination of both. In the LHS, different prograde

path styles have been attributed to single vs. multiple thrusting episodes [Catlos *et al.*, 2001; Kohn *et al.*, 2001]. These site-specific tectonic interpretations tend to emphasize the role of vertical heat transport [e.g., England and Thompson, 1984], and may be difficult to reconcile with other data from the orogen.

Results from HT1 show that a variety of different P - T - t path styles can be produced simultaneously in different parts of the model orogen with no change in tectonic boundary conditions (Fig. 4b, 6b, 12e). The observed styles include near-isothermal decompression (G1, E1, E2), cooling during decompression (G1-G4, L1-L4), near-isobaric heating (G2, G3, G4, L4), and hairpins (L1, L2). The material points recording these paths have been juxtaposed at the orogenic front only at the end of the model (Fig. 8d). All the P - T paths produced by this model are normal loops ('clockwise' in the P -up graphical reference frame), with P_{max} reached before T_{max} , consistent with most P - T - t paths reported from the Himalaya. The model does not produce reverse ('counter-clockwise') loops, where T_{max} is reached before P_{max} [cf. Goscombe and Hand, 2000].

In model HT1, near-isothermal decompression is recorded at lower structural levels in the "GHS" and near-isobaric heating at higher structural levels. In petrological studies, isothermal decompression is generally interpreted to indicate rapid exhumation [e.g., Spear, 1993; Ring *et al.*, 1999]. Although clearly valid in many cases, the present study shows that this is not the only possible interpretation. In the model, isothermal decompression is associated with pro-ward translation of points that have been entrained in the deep, high-temperature region of the channel, where they experience gradually declining pressure at nearly constant temperature (Fig. 3). In contrast, isobaric heating occurs in the upper part of the channel and overlying middle crust, where material heats up by radioactive self-heating at the same time that it is translated outward at nearly constant depth beneath the plateau. This simple pattern could be modified by upper

crustal extension between the erosion front and the suture [Beaumont *et al.*, 2004], leading to steep decompression paths in the immediately underlying channel.

Throughout the model "GHS", rapid exhumation in the last 5-10 My of the model is accompanied by both cooling and decompression, and the resulting retrograde P - T - t paths are characterized by moderate, rather than steep, dP/dT slopes (Fig. 4c, 6c). Similar retrograde paths observed in some parts of the GHS have been explained in terms of post-peak cooling during decompression along a 'constant geothermal gradient' [e.g., Vannay and Grasemann, 1998]. However, geotherms vary with space and time across the model orogenic front throughout its evolution (Fig. 3) and constant geotherms should not be expected in similar settings in nature.

Hairpin P - T - t paths, where T_{max} and P_{max} approximately coincide, are associated with "LHS" points that are exhumed shortly after their initial burial as the orogen propagates into its foreland, and which therefore have a very short residence time within the model orogen. The range of "LHS" path styles, from hairpins (L1, L2) to various degrees of near-isobaric heating (L4) or heating during decompression (L3) reflect the degree to which the points are carried beneath the orogen before the onset of exhumation, and thus duration of burial and proximity to the overlying hot channel.

These results demonstrate the dominance of lateral over vertical transport of material points that emerge at the model surface together. As the model orogen evolves, material moves through different tectonic and thermal regimes that exist simultaneously in different parts of the system. The resulting P - T paths reflect how specific points (Lagrangian reference frame) have traveled through the orogen as a whole (Eulerian reference frame) [e.g., Fulsack, 1995; Beaumont *et al.*, 2004]. This model prediction is difficult to test because it is generally impossible to estimate lateral transport distances from rocks in which deformation and metamorphism have largely obliterated evidence of original provenance and distribution. Structural reconstructions provide

only minimum constraints on original separation [e.g., *Searle, 1999; DeCelles et al., 2002; Searle et al., 2003*], and protolith boundaries inferred from contrasting lithologies [e.g., *Grujic et al., 1996*] or isotopic data [*Parrish and Hodges, 1996; DeCelles et al., 2000; Myrow et al., 2003*] are compatible with lateral transport but provide no quantitative estimates of its amount.

10.3. Diachronous vs. discrete metamorphic "events"

In most metamorphic belts including the Himalaya, overprinting metamorphic assemblages are interpreted in terms of a sequence of discrete metamorphic events [e.g., M1, M2; *Hodges et al., 1988*], normally inferred to represent different tectonic or thermal regimes that affected a specific volume of crust at different times. The present study suggests an alternative view - that overprinting assemblages may represent lateral transport of rocks through contrasting thermal-tectonic regimes that existed simultaneously in different parts of the orogen. Here we interpret the M1 metamorphism to represent the time at which points transported into the orogen in the early stages of collision reached their maximum burial depth ($t@P_{max}$; Fig. 9b) and began to travel outwards with the channel flow. The lower pressure M2 'overprint' represents the time at which the same points reached their maximum temperature ($t@T_{max}$; Fig. 9b) during lateral transit beneath the plateau. According to this view, the conditions that produced the Eohimalayan (M1) metamorphism at ca. 28-36 Ma and the Neohimalayan (M2) metamorphism at ca. 20-24 Ma could still exist today beneath the southern Tibetan plateau. The discrete age populations that characterize these 'events' in the present-day Himalaya were recorded by rocks that traveled through corresponding parts of the orogen at these particular times. Their equivalents are forming today and will eventually emerge at the orogenic front if channel flow and surface denudation continue to operate as they have in the past.

Likewise, the model predicts that leucogranites should have been produced since the onset of partial melting and channel flow at ca. 30 Ma. Plutons formed at ca. 20-25 Ma have now

reached the erosion front; older plutons have already been eroded and younger ones are only locally exposed [e.g., *Wu et al.*, 1998; *Grujic et al.*, 2002]. Despite the large lateral transport distances, the subsurface position of the model suture (Fig. 2d, 3d) and material tracking in HT1 [*Beaumont et al.*, 2004] indicate that retro-side ("Asian") material entrained in the channel is still ca. 200 km north of the erosion front. The model therefore predicts that metamorphic rocks and leucogranites now exposed in the Himalaya and southern Tibet (south of the Indus-Tsangpo suture) should have Indian crustal protoliths.

10.4. A cautionary note

In this paper we have tested a variety of predictions from a single representative model against a variety of data, mainly from Nepal, the best-known part of the orogen. The most important constraints on the model are crustal-scale structure and tectonic style, geochronology, orogen-scale patterns of metamorphism, and erosion rates. The generally good correspondence between model predictions and a range of independent observations gives us confidence that, to a first approximation, model HT1 provides a plausible explanation for the first-order features of the Himalayan-Tibetan orogen. Improved lithosphere-scale seismic data, integrated erosion and unroofing histories, well constrained P - T - t paths and cross-sections from a range of representative transects, and additional constraints on protolith provenance would be particularly useful for refining and testing future models.

An alternative approach would be to compare results from a number of different models [e.g., *Beaumont et al.*, 2004] with a specific type of data (e.g., peak grade profiles) from one or more natural transects, in order to find the model parameters that provide the best fit to the observations. For example, different combinations of erosion histories and upper crustal strengths could be tested against cooling ages to refine the denudation model. We have chosen not to do this here because, as demonstrated by *Beaumont et al.* [2004], significant variations in

model style in the vicinity of the erosion front can be produced by parameters that vary within the range allowed by existing constraints from the Himalayan-Tibetan system. Furthermore, the present generation of models lacks the necessary spatial resolution for detailed comparisons and does not include some potentially important effects, such as shear heating, strain localization, and out-of-plane flow, that could significantly affect model predictions on the scale of individual transects. Conversely, the inherent variability in the natural system (e.g., lithologies, precipitation) would limit the general applicability of any model tuned to fit the data from any one transect. Therefore, although we expect the model results reported here to be applicable to the first-order tectonic and metamorphic features of the Himalaya and southern Tibet, we caution against using results from model HT1 to explain specific details of any particular transect.

11. Conclusions

Results from a thermal-mechanical numerical model (HT1) in which channel flow, driven by a topographically-induced differential pressure operating on thermally weakened middle crust, is coupled with focused surface denudation, are compatible with a range of metamorphic and geochronological data from the Himalayan-Tibetan system. Model P - T paths and peak grade profiles are generally compatible with metamorphic P - T data from the central part of the orogen. Model predictions agree well with peak metamorphic ages from both the GHS and LHS and with LHS cooling ages; predicted GHS cooling ages are 5-10 My too young. Erosion of model metamorphic facies is consistent with observed detrital mineral assemblages. The model also provides an explanation for lower crustal eclogite that is strongly overprinted by granulite, like that present in the eastern Himalaya. We conclude that models of this type offer a plausible explanation for metamorphism in the Himalayan-Tibetan orogen.

The inverted metamorphism associated with the MCT is interpreted to result from the combined effects of distributed ductile shear within the MCT zone and extrusion of the hot GHS channel above the LHS. The range of P - T path styles produced by the model, which resembles the range observed in the Himalaya, reflects material transport through contrasting P - T regimes that exist simultaneously in different parts of model. Contrary to some conventional interpretations, the present work shows that isothermal decompression paths do not necessarily require rapid exhumation, and isobaric heating paths do not require post-thrusting thermal relaxation. In the model, these path styles result from lateral transport at different levels in the hot channel as it flows outward beneath the plateau. In contrast, hairpin paths reflect a short residence time beneath the flank of the propagating orogen.

The close correspondence between the observed times of Himalayan M1 and M2 metamorphic 'events' and model $t@P_{max}$ and $t@T_{max}$, respectively, suggests that M1 represents the time at which GHS material now at the surface was entrained with the outward flowing channel, whereas M2 corresponds to the time of maximum heating as the channel material approached the plateau flank. In the model, this is also the time at which some "GHS" P - T paths intersect the muscovite dehydration melting field. According to this view, these times do not mark discrete events associated with orogen-scale changes in tectonic or thermal conditions but are 'snapshots' of a continuous process that may still be operating today. Finally, we conclude that lateral transport of heat and material dominates over vertical transport in large, hot orogens like the Himalayan-Tibetan system, especially where conditions are favorable for channel flow.

Acknowledgments: This work is dedicated to the memory of Doug Nelson, who challenged us to produce model results compatible with observations from the Himalayan-Tibetan orogen. The research was funded by Natural Sciences and Engineering Research Council and Lithoprobe

Supporting Geoscience grants to RAJ and CB. CB has also been supported by the Inco Fellowship of the Canadian Institute for Advanced Research, and by the Canada Research Chairs programme. The models were developed and run with the assistance of Phillippe Fullsack and Bonny Lee. The work has benefited greatly from discussions with many colleagues, including Doug Nelson, Djordje Grujic, and Yani Najman. Constructive reviews by Linc Hollister, Kip Hodges, and Jean Braun significantly improved the final version of this paper.

References

- Batt, G.E., and J. Braun, On the thermo-mechanical evolution of compressional orogens, *Geophysical Journal International*, 128, 364-382, 1997.
- Beaumont, C., R.A. Jamieson, M.H. Nguyen, and B. Lee, Himalayan tectonics explained by extrusion of a low-viscosity channel coupled to focused surface denudation, *Nature*, 414, 738-742, 2001a.
- Beaumont, C., R.A. Jamieson, M.H. Nguyen, and B. Lee, Mid-crustal channel flow in large hot orogens: results from coupled thermal-mechanical models, in *Slave - Northern Cordillera Lithospheric Evolution (SNORCLE) and Cordilleran Tectonics Workshop; Report of 2001 Combined Meeting, Lithoprobe Report*, compiled by F. Cook and P. Erdmer, pp. 112-170, 2001b.
- Beaumont, C., R.A. Jamieson, M.H. Nguyen, and S. Medvedev, Crustal exhumation and doming mechanisms in large hot orogens: Numerical models and comparison with observations, *Geological Association of Canada, Abstracts*, 28, 9, 2003.
- Beaumont, C., R.A. Jamieson, M.H. Nguyen, and S. Medvedev, Crustal channel flows: 1. Numerical models with applications to the tectonics of the Himalayan-Tibetan Orogen, *Journal of Geophysical Research*, this volume, 2004.
- Brewer, I.D., D.W. Burbank, and K.V. Hodges, Modelling detrital cooling-age populations: Insights from two Himalayan catchments, *Basin Research*, 15, 305-320, 2003.
- Brunel, M., and J-R. Kienast, Étude pétro-structurale des chevauchements ductiles himalayens sur la transversale de l'Everest - Makalu (Népal-orientale), *Canadian Journal of Earth Sciences*, 23, 1117-1137, 1986.
- Burbank, D.W., J. Leland, E. Fielding, R.S. Anderson, N. Brozovic, M.R. Reid, and C. Duncan, Bedrock incision, rock uplift, and threshold hillslopes in the northwestern Himalayas, *Nature*, 379, 505-510, 1996.

- Burchfiel, B.C., Z. Chen, K.V. Hodges, Y. Liu, L.H. Royden, C. Deng, and J. Xu, The South Tibetan detachment system, Himalayan orogen: Extension contemporaneous with and parallel to shortening in a collisional mountain belt, *Geological Society of America, Special Paper*, 269, 41 pp., 1992.
- Burchfiel, B.C., and L.H. Royden, North-south extension within the convergent Himalayan region, *Geology*, 13, 679-682, 1985.
- Burg, J-P., M. Brunel, D. Gapais, G. Chen, and G.H. Liu, Deformation of leucogranites of the crystalline Main Central Sheet in southern Tibet (China), *Journal of Structural Geology*, 6, 535-542, 1984.
- Catlos, E.J., T.M. Harrison, M.J. Kohn, M. Grove, F.J. Ryerson, C.E. Manning, and B.N. Upreti, Geochronologic and thermobarometric constraints on the evolution of the Main Central Thrust, central Nepal Himalaya, *Journal of Geophysical Research*, 106, 16177-16204, 2001.
- Clark, M.K., and L.H. Royden, Topographic ooze: Building the eastern margin of Tibet by lower crustal flow, *Geology*, 28, 703-706, 2000.
- Coleman, M.E., Orogen-parallel and orogen-perpendicular extension in the central Nepalese Himalayas, *Geological Society of America Bulletin*, 108, 1594-1607, 1996.
- Coleman, M.E., U-Pb constraints on Oligocene-Miocene deformation and anatexis within the central Himalayas, Marsyandi Valley, Nepal, *American Journal of Science*, 298, 553-571, 1998.
- Copeland, P., and T.M. Harrison, Episodic rapid uplift in the Himalaya revealed by $^{40}\text{Ar}/^{39}\text{Ar}$ analysis of detrital K-feldspar and muscovite, Bengal Fan, *Geology*, 18, 354-357, 1990.
- Copeland, P., T.M. Harrison, K.V. Hodges, P. Maruejol, P. LeFort, and A. Pecher, An Early Pliocene thermal disturbance of the Main Central Thrust, central Nepal: Implications for Himalayan tectonics, *Journal of Geophysical Research*, 96, 8475-8500, 1991.
- Craw, D., Fluid evolution during uplift of the Annapurna Himal, central Nepal, *Lithos*, 24, 137-150, 1990.
- Daniel, C.G., L.S. Hollister, R.R. Parrish, and D. Grujic, Exhumation of the Main Central Thrust zone from lower crustal depths, eastern Bhutan Himalaya, *Journal of Metamorphic Geology*, 21, 317-334, 2003.
- Davidson, C., D. Grujic, L.S. Hollister, and S.M. Schmid, Metamorphic reactions related to decompression and synkinematic intrusion of leucogranite, High Himalayan Crystallines, Bhutan, *Journal of Metamorphic Geology*, 15, 593-612, 1997.
- de Sigoyer, J., V. Chavagnac, J. Blichert-Toft, I.M. Villa, B. Luais, S. Cuillot, M. Cosca, and G. Mascle, Dating the Indian continental subduction and collisional thickening in the northwest Himalaya: Multichronology of the Tso Moriri eclogites, *Geology*, 28, 487-490, 2000.

- DeCelles, P.G., G.E. Gehrels, J. Quade, B. LaReau, and M. Spurlin, Tectonic implications of U-Pb zircon ages of the Himalayan orogenic belt in Nepal, *Science*, 288, 497-499, 2000.
- DeCelles, P.G., G.E. Gehrels, J. Quade, T.P. Ojha, P.A. Kapp, and B.N. Upreti, Neogene foreland deposits, erosional unroofing, and the kinematic history of the Himalayan fold-thrust belt, western Nepal, *Geological Society of America Bulletin*, 110, 2-21, 1998.
- DeCelles, P.G., D.M. Robinson, and G. Zandt, Implications of shortening in the Himalayan fold-thrust belt for uplift of the Tibetan Plateau, *Tectonics*, 21 (1062), doi:10.1029/2001TC001322, 2002.
- Ducea, M.N., V. Lutkov, V.T. Minaev, B. Hacker, L. Ratschbacher, P. Luffi, M. Schwab, G.E. Gehrels, M. McWilliams, J. Vervoort, and J. Metcalf, Building the Pamirs: The view from the underside, *Geology*, 21, 849-852, 2003.
- Duncan, C., J. Masek, and E. Fielding, How steep are the Himalaya? Characteristics and implications of along-strike topographic variations, *Geology*, 31, 75-78, 2003.
- Edwards, M.A., and T.M. Harrison, When did the roof collapse? Late Miocene north-south extension in the high Himalaya revealed by Th-Pb monazite dating of the Khula Kangri granite, *Geology*, 25, 543-546, 1997.
- England, P.C., and P. Molnar, The interpretation of inverted metamorphic isograds using simple physical calculations, *Tectonics*, 12, 145-157, 1993.
- England, P.C., and A.B. Thompson, Pressure-temperature-time paths of regional metamorphism I. Heat transfer during the evolution of regions of thickened continental crust, *Journal of Petrology*, 25, 894-928, 1984.
- Finlayson, D.P., D.R. Montgomery, and B. Hallet, Spatial coincidence of rapid inferred erosion with young metamorphic massifs in the Himalayas, *Geology*, 30, 219-222, 2002.
- France-Lanord, C., L. Derry, and A. Michard, Evolution of the Himalaya since Miocene time: Isotopic and sedimentological evidence from the Bengal Fan, in *Himalayan Tectonics*, edited by P.J. Treloar, and M.P. Searle, pp. 603-621, *Geological Society Special Publication*, 74, 1993.
- Fraser, G., B. Worley, and M. Sandiford, High-precision geothermobarometry across the High Himalayan metamorphic sequence, Langtang Valley, Nepal, *Journal of Metamorphic Geology*, 18, 665-682, 2000.
- Fullsack, P., An arbitrary Lagrangian-Eulerian formulation for creeping flows and its application in tectonic models, *Geophysical Journal International*, 120, 1-23, 1995.
- Galy, A., and C. France-Lanord, Higher erosion rate in the Himalaya: Geochemical constraints on riverine fluxes, *Geology*, 29, 23-26, 2001.

- Gleason, G.C., and J. Tullis, A flow law for dislocation creep of quartz aggregates determined with the molten salt cell, *Tectonophysics*, 247, 1-23, 1995.
- Godin, L., R.R. Parrish, R.L. Brown, and K.V. Hodges, Crustal thickening leading to exhumation of the Himalayan metamorphic core of central Nepal: Insight from U-Pb geochronology and $^{40}\text{Ar}/^{39}\text{Ar}$ thermochronology, *Tectonics*, 20, 729-747, 2001.
- Goscombe, B., and M. Hand, Contrasting P-T paths in the eastern Himalaya, Nepal: Inverted isograds in a paired metamorphic mountain belt, *Journal of Petrology*, 41, 1673-1719, 2000.
- Grove, M., and T.M. Harrison, Monazite Th-Pb age depth profiling, *Geology*, 27, 487-490, 1999.
- Grujic, D., M. Casey, C. Davidson, L.S. Hollister, R. Kundig, T. Pavlis, and S. Schmid, Ductile extrusion of the Higher Himalayan Crystalline in Bhutan: Evidence from quartz microfabrics, *Tectonophysics*, 260, 21-43, 1996.
- Grujic, D., L.S. Hollister, and R.R. Parrish, Himalayan metamorphic sequence as an orogenic channel: Insight from Bhutan, *Earth and Planetary Science Letters*, 198, 177-191, 2002.
- Guillot, S., M. Cosca, P. Allemand, and P. LeFort, Contrasting metamorphic and geochronologic evolution along the Himalayan belt, in *Himalaya and Tibet: Mountain Roots to Mountain Tops*, edited by A. Macfarlane, R.B. Sorkhabi, and J. Quade, pp. 117-128, *Geological Society of America, Special Paper*, 328, 1999.
- Guillot, S., P. LeFort, A. Pecher, M.R. Barman, and J. Arahamian, Contact metamorphism and depth of emplacement of the Manaslu granite (central Nepal): Implications for Himalayan orogenesis, *Tectonophysics*, 241, 99-119, 1995.
- Hacker, B.R., E. Gnos, L. Ratschbacher, M. Grove, M. McWilliams, S.V. Sobolev, J. Wan, and W. Zhenhan, Hot and dry deep crustal xenoliths from Tibet, *Science*, 287, 2463-2466, 2000.
- Haines, S.S., S.L. Klemperer, L. Brown, J. Guo, J. Mechie, R. Meissner, A. Ross, and W. Zhao, INDEPTH III seismic data: From surface observations to deep crustal processes in Tibet, *Tectonics*, 22 (1001), doi:10.1029/2001TC001305, 2003.
- Harrison, T.M., M. Grove, O.M. Lovera, and E. Catlos, A model for the origin of Himalayan anatexis and inverted metamorphism, *Journal of Geophysical Research*, 103, 27017-27032, 1998.
- Harrison, T.M., M. Grove, K.D. McKeegan, C.D. Coath, O.M. Lovera, and P. LeFort, Origin and episodic emplacement of the Manaslu intrusive complex, central Himalaya, *Journal of Petrology*, 40, 3-19, 1999.
- Harrison, T.M., K.D. McKeegan, and P. LeFort, Detection of inherited monazite in the Manaslu leucogranite by $^{208}\text{Pb}/^{232}\text{Th}$ ion microprobe dating: Crystallization age and tectonic implications, *Earth and Planetary Science Letters*, 133, 271-282, 1995.

- Harrison, T.M., F.J. Ryerson, P. LeFort, A. Yin, O.M. Lovera, and E.J. Catlos, A Late Miocene-Pliocene origin for the central Himalayan inverted metamorphism, *Earth and Planetary Science Letters*, 146, E1-E7, 1997.
- Hauck, M.L., K.D. Nelson, L.D. Brown, W. Zhao, and A.R. Ross, Crustal structure of the Himalayan orogen at ~90° east longitude from Project INDEPTH deep reflection profiles, *Tectonics*, 17, 481-500, 1998.
- Henry, P., X. Le Pichon, and B. Goffé, Kinematic, thermal and petrological model of the Himalayas: Constraints related to metamorphism within the underthrust Indian crust and topographic elevation, *Tectonophysics*, 273, 31-56, 1997.
- Hodges, K.V., Tectonics of the Himalaya and southern Tibet from two perspectives, *Geological Society of America Bulletin*, 112, 324-350, 2000.
- Hodges, K.V., B.C. Burchfiel, L.H. Royden, Z. Chen, and Y. Liu, The metamorphic signature of contemporaneous extension and shortening in the central Himalayan orogen: Data from the Nyalam transect, southern Tibet, *Journal of Metamorphic Geology*, 11, 721-737, 1993.
- Hodges, K.V., W.E. Hames, W. Olszewski, B.C. Burchfiel, L.H. Royden, and Z. Chen, Thermobarometric and $^{40}\text{Ar}/^{39}\text{Ar}$ geochronologic constraints on Eohimalayan metamorphism in the Dinggye area, southern Tibet, *Contributions to Mineralogy and Petrology*, 117, 151-163, 1994.
- Hodges, K.V., M.S. Hubbard, and D.S. Silverberg, Metamorphic constraints on the thermal evolution of the central Himalayan orogen, *Philosophical Transactions, Royal Society of London*, A326, 257-280, 1988.
- Hodges, K.V., J.M. Hurtado, and K.X. Whipple, Southward extrusion of Tibetan crust and its effect on Himalayan tectonics, *Tectonics*, 20, 799-809, 2001.
- Hodges, K.V., R.R. Parrish, T.B. Housh, D.R. Lux, B.C. Burchfiel, L.H. Royden, and Z. Chen, Simultaneous Miocene extension and shortening in the Himalayan orogen, *Science*, 258, 1466-1470, 1992.
- Hodges, K.V., R.R. Parrish, and M.P. Searle, Tectonic evolution of the central Annapurna range, Nepalese Himalaya, *Tectonics*, 15, 1264-1291, 1996.
- Holdaway, M.J., Stability of andalusite and the aluminum silicate phase diagram, *American Journal of Science*, 271, 97-131, 1971.
- Hollister, L.S., The role of melt in the uplift and exhumation of orogenic belts, *Chemical Geology*, 108, 31-48, 1993.
- Hubbard, M.S., Ductile shear as a cause of inverted metamorphism: Example from the Nepal Himalaya, *Journal of Geology*, 104, 493-499, 1996.

- Hubbard, M.S., Thermobarometric constraints on the thermal history of the Main Central Thrust zone and Tibetan Slab, eastern Nepal Himalaya, *Journal of Metamorphic Geology*, 7, 127-134, 1989.
- Huerta, A.D., L.H. Royden, and K.V. Hodges, The thermal structure of collisional orogens as a response to accretion, erosion, and radiogenic heating, *Journal of Geophysical Research*, 103, 15287-15302, 1998.
- Huerta, A.D., L.H. Royden, and K.V. Hodges, The effects of accretion, erosion and radiogenic heat on the metamorphic evolution of collisional orogens, *Journal of Metamorphic Geology*, 17, 349-366, 1999.
- Inger, S., and N.B.W. Harris, Tectonothermal evolution of the High Himalayan Crystalline Sequence, Langtang Valley, northern Nepal, *Journal of Metamorphic Geology*, 10, 439-452, 1992.
- Jain, A.K., and R.M. Manickavasagam, Inverted metamorphism in the intracontinental ductile shear zone during Himalayan collision tectonics, *Geology*, 21, 407-410, 1993.
- Jamieson, R.A., C. Beaumont, P. Fullsack, and B. Lee, Barrovian regional metamorphism: Where's the heat?, in *What Drives Metamorphism and Metamorphic Reactions?*, edited by P.J. Treloar and P. O'Brien, pp. 23-45, *Geological Society Special Publication*, 138, 1998.
- Jamieson, R.A., C. Beaumont, J. Hamilton, and P. Fullsack, Tectonic assembly of inverted metamorphic sequences, *Geology*, 24, 839-842, 1996.
- Jamieson, R.A., C. Beaumont, M.H. Nguyen, and B. Lee, Interaction of metamorphism, deformation, and exhumation in large convergent orogens, *Journal of Metamorphic Geology*, 20, 1-16, 2002.
- Johnson, M.R.W., Shortening budgets and the role of continental subduction during the India-Asia collision, *Earth Science Reviews*, 59, 101-123, 2002.
- Ketchum, J.W.F. and A. Davidson, Crustal architecture and tectonic assembly of the Central Gneiss Belt, southwestern Grenville Province, Canada: A new interpretation, *Canadian Journal of Earth Sciences*, 37, 217-234, 2000
- Kohn, M.J., E.J. Catlos, F.J. Ryerson, and T.M. Harrison, Pressure-temperature-time path discontinuity in the Main Central Thrust zone, central Nepal, *Geology*, 29, 571-574, 2001.
- Koons, P.O., P.K. Zeitler, C.P. Chamberlain, D. Craw, and A.S. Meltzer, Mechanical links between erosion and metamorphism in Nanga Parbat, Pakistan Himalaya, *American Journal of Science*, 302, 749-773, 2002.
- LeFort, P., Himalaya: the collided range. Present knowledge of the continental arc, *American Journal of Science*, 275A, 1-44, 1975.

- Lombardo, B., and F. Rolfo, Two contrasting eclogite types in the Himalayas: Implications for the Himalayan orogeny, *Journal of Geodynamics*, 30, 37-60, 2000
- Macfarlane, A.M., An evaluation of the inverted metamorphic gradient at Langtang National Park, central Nepal Himalaya, *Journal of Metamorphic Geology*, 13, 595-612, 1995.
- Mackwell, S.J., M.E. Zimmerman, and D.L. Kohlstedt, High-temperature deformation of dry diabase with application to tectonics on Venus, *Journal of Geophysical Research*, 103, 975-984, 1998.
- Mahéo, G., S. Guillot, J. Blichert-Toft, Y. Rolland, and A. Pêcher, A slab breakoff model for the Neogene thermal evolution of South Karakoram and South Tibet, *Earth and Planetary Science Letters*, 195, 15-58, 2002.
- Mancktelow, N., Nonlithostatic pressure during sediment subduction and the development and exhumation of high pressure metamorphic rocks, *Journal of Geophysical Research*, 100, 571-583, 1995.
- Mecklenburgh, J., and E.H. Rutter, On the rheology of partially molten synthetic granite, *Journal of Structural Geology*, 25, 1575-1585, 2003.
- Medvedev, S., C. Beaumont, O. Vanderhaeghe, P. Fullsack, and R.A. Jamieson, Evolution of continental plateaus: Insights from thermal-mechanical modelling, *EOS, Transactions of the American Geophysical Union*, 81, F1094, 2000.
- Molnar, P., and P. England, Temperatures, heat flux, and frictional stress near major thrust faults, *Journal of Geophysical Research*, 95, 4833-4856, 1990.
- Molnar, P., P. England, and J. Martinod, Mantle dynamics, uplift of the Tibetan plateau, and the Indian monsoon, *Reviews of Geophysics*, 31, 357-396, 1993.
- Myrow, P.M., N.C. Hughes, T.S. Paulsen, I.S. Williams, S.K. Parcha, K.R. Thompson, S.A. Bowring, S-C. Peng, and A.D. Ahluwalia, Integrated tectonostratigraphic analysis of the Himalaya and implications for its tectonic reconstruction, *Earth and Planetary Science Letters*, 212, 433-441, 2003.
- Najman, Y., and E. Garzanti, Reconstructing early Himalayan tectonic evolution and paleogeography from Tertiary foreland basin sediments, northern India, *Geological Society of America Bulletin*, 112, 435-449, 2000.
- Najman, Y., E. Garzanti, M. Pringle, M. Bickle, D. Burbank, S. Ando, and N. Brozovic, Exhumation and attainment of steady state in the Himalaya: Insights from the detrital sediment record, *EOS, Transactions of the American Geophysical Union*, 89, F1302, 2002
- Nelson, K.D., W. Zhao, L.D. Brown, J. Kuo, J. Che, X. Liu, S.L. Klemperer, Y. Makovsky, R. Meissner, J. Mechie, R. Kind, F. Wenzel, J. Ni, J. Nabelek, L. Chen, H. Tan, W. Wei, A.G.

- Jones, J. Booker, M. Unsworth, W.S.F. Kidd, M. Hauck, D. Alsdorf, A. Ross, M. Cogan, C. Wu, E.A. Sandvol, and M. Edwards, Partially molten middle crust beneath southern Tibet; synthesis of Project INDEPTH results, *Science*, 274 (5293), 1684-1688, 1996.
- O'Brien, P.J., N. Zotov, R. Law, M.A. Khan, and M.Q. Jan, Coesite in Himalayan eclogite and implications for models of India-Asia collision, *Geology*, 29, 435-438, 2001.
- Oxburgh, E.R., and D.L. Turcotte, Thermal gradients and regional metamorphism in overthrust terrains with special reference to the eastern Alps, *Schweizerische Mineralogische und Petrographische Mitteilungen*, 54, 641-662, 1970.
- Parrish, R.R., and K.V. Hodges, Isotopic constraints on the age and provenance of the Lesser and Greater Himalayan sequences, Nepalese Himalaya, *Geological Society of America Bulletin*, 108, 904-911, 1996.
- Pattison, D.R.M., Stability of andalusite and sillimanite and the Al_2SiO_5 triple point: Constraints from the Ballachulish aureole, Scotland, *Journal of Geology*, 100, 423-446, 1992.
- Pognante, U., and D.A. Spencer, First report of eclogites from the Himalayan belt, Kaghan Valley (northern Pakistan), *European Journal of Mineralogy*, 3, 613-618, 1991.
- Pope, D.C., and S.D. Willett, Thermal-mechanical model for crustal thickening in the Central Andes driven by ablative subduction, *Geology*, 26, 511-514, 1998.
- Ring, U., M.T. Brandon, S.D. Willett, and G.S. Lister, Exhumation processes, in *Exhumation Processes: Normal Faulting, Ductile Flow, and Erosion*, edited by U. Ring, M.T. Brandon, G.S. Lister, and S.D. Willett, pp. 1-27, *Geological Society Special Publication*, 154, 1999.
- Robinson, D.M., P.G. DeCelles, C.N. Garzione, O.N. Pearson, T.M. Harrison, and E.J. Catlos, Kinematic model for the Main Central Thrust in Nepal, *Geology*, 31, 359-362, 2003.
- Rolland, Y., G. Maheo, S. Guillot, and A. Pecher, Tectono-metamorphic evolution of the Karakorum metamorphic complex (Dassu-Askole area, NE Pakistan): Exhumation of mid-crustal HT-MP gneisses in a convergent context, *Journal of Metamorphic Geology*, 19, 717-737, 2001.
- Royden, L.H., The steady-state thermal structure of eroding orogenic belts and accretionary prisms, *Journal of Geophysical Research*, 98, 4487-4507, 1993.
- Royden, L.H., Coupling and decoupling of crust and mantle in convergent orogens: Implications for strain partitioning in the crust, *Journal of Geophysical Research*, 101, 17679-17705, 1996.
- Royden, L.H., B.C. Burchfiel, R.W. King, Z. Chen, F. Shen, and Y. Liu, Surface deformation and lower crustal flow in eastern Tibet, *Science*, 276, 788-790, 1997.
- Ruppel, C., and K.V. Hodges, Pressure-temperature-time paths from two-dimensional thermal

- models: Prograde, retrograde, and inverted metamorphism, *Tectonics*, *13*, 17-44, 1994.
- Rushmer, T., Volume change during partial melting reactions: Implications for melt extraction, melt geochemistry and crustal rheology, *Tectonophysics*, *342*, 389-403, 2001.
- Schärer, U., The effect of initial ^{230}Th disequilibrium on young U-Pb ages: The Makalu case, *Earth and Planetary Science Letters*, *67*, 191-204, 1984.
- Schärer, U., R.H. Xu, and C.J. Allegre, U-[Th]-Pb systematics and ages of Himalayan leucogranites, south Tibet, *Earth and Planetary Science Letters*, *77*, 35-48, 1986.
- Searle, M.P., Cooling history, erosion, exhumation, and kinematics of the Himalaya-Karakoram-Tibet orogenic belt, in *Tectonics of Asia*, edited by A. Yin and T.M. Harrison, pp. 110-137, Cambridge University Press, 1996.
- Searle, M.P., Extensional and compressional faults in the Everest - Lhotse massif, Khumbu Himalaya, Nepal, *Journal of the Geological Society*, *156*, 227-240, 1999.
- Searle, M.P., and L. Godin, The south Tibetan detachment and the Manaslu leucogranite: A structural reinterpretation and restoration of the Annapurna-Manaslu Himalaya, Nepal, *Journal of Geology*, *111*, 505-523, 2003.
- Searle, M.P., S.R. Noble, A.J. Hurford, and D.C. Rex, Age of crustal melting, emplacement, and exhumation history of the Shivling leucogranite, Garwhal Himalaya, *Geological Magazine*, *136*, 513-525, 1999a.
- Searle, M.P., R.R. Parrish, K.V. Hodges, A. Hurford, M.W. Ayres, and M.J. Whitehouse, Shisha Pangma leucogranite, South Tibetan Himalaya: Field relations, geochemistry, age, origin, and emplacement, *Journal of Geology*, *105*, 307-326, 1997.
- Searle, M.P., and A.J. Rex, Thermal model for the Zaskar Himalaya, *Journal of Metamorphic Geology*, *7*, 127-134, 1989.
- Searle, M.P., R.L. Simpson, R.D. Law, R.R. Parrish, and D.J. Waters, The structural geometry, metamorphic and magmatic evolution of the Everest massif, High Himalaya of Nepal - South Tibet, *Journal of the Geological Society*, *160*, 345-366, 2003.
- Searle, M.P., D.J. Waters, M.W. Dransfield, B.J. Stephenson, C.B. Walker, J.D. Walker, and D.C. Rex, Thermal and mechanical models for the structural and metamorphic evolution of the Zaskar High Himalaya, in *Continental Tectonics*, edited by C. MacNiocaill and P.D. Ryan, pp. 139-156, *Geological Society Special Publication*, *164*, 1999b.
- Shen, F., L.H. Royden, and B.C. Burchfiel, Large-scale crustal deformation of the Tibetan Plateau, *Journal of Geophysical Research*, *106*, 6793-6816, 2001.
- Simpson, R.L., R.R. Parrish, M.P. Searle, and D.J. Waters, Two episodes of monazite crystallization during metamorphism and crustal melting in the Everest region of the

- Nepalese Himalaya, *Geology*, 28, 403-406, 2000.
- Spear, F.S., *Metamorphic Phase Equilibria and Pressure-Temperature-Time Paths*, 799 pp, Mineralogical Society of America, Monograph, 1993.
- Swapp, S.M., and L.S. Hollister, Inverted metamorphism within the Tibetan slab of Bhutan: Evidence for a tectonically transported heat-source, *Canadian Mineralogist*, 29, 1019-1041, 1991.
- Treloar, P.J., P.J. O'Brien, R.R. Parrish, and M.A. Khan, Exhumation of early Tertiary, coesite-bearing eclogites from the Pakistan Himalaya, *Journal of the Geological Society*, 160, 367-376, 2003.
- Turcotte, D.L., and G. Schubert, *Geodynamics: Applications of Continuum Physics to Geological Problems*, 450 pp., John Wiley and Sons, 1982.
- Vance, D., and N. Harris, Timing of prograde metamorphism in the Zaskar Himalaya, *Geology*, 27, 395-398, 1999.
- Vance, D., and E. Mahar, Pressure-temperature paths from P-T pseudosections and zoned garnets: Potential, limitations and examples from the Zaskar Himalaya, NW India, *Contributions to Mineralogy and Petrology*, 132, 225-245, 1998.
- Vanderhaeghe, O., S. Medvedev, P. Fullsack, C. Beaumont, and R.A. Jamieson, Evolution of orogenic wedges and continental plateaux: Insights from crustal thermal-mechanical models overlying subducting mantle lithosphere, *Geophysical Journal International*, 153, 27-51, 2003.
- Vannay, J.-C., and B. Grasemann, Himalayan inverted metamorphism and syn-convergence extension as a consequence of a general shear extrusion, *Geological Magazine*, 138, 253-276, 2001.
- Vannay, J.-C., and B. Grasemann, Inverted metamorphism in the High Himalaya of Himachal Pradesh (NW India): Phase equilibria versus thermobarometry, *Schweizerische Mineralogische und Petrographische Mitteilungen*, 78, 107-132, 1998.
- Vannay, J.-C., B. Grasemann, M.Rahn, W. Frank, A. Carter, V. Baudraz, and M. Cosca, Miocene to Holocene exhumation of metamorphic crustal wedges in the NW Himalaya: Evidence for tectonic extrusion coupled to fluvial erosion, *Tectonics*, 23, TC1014, doi:10.1029/2002TC001429, 2004.
- Vannay, J.-C., and K.V. Hodges, Tectonometamorphic evolution of the Himalayan metamorphic core between the Annapurna and Dhauligiri, central Nepal, *Journal of Metamorphic Geology*, 14, 635-656, 1996.
- Viskupic, K., and K.V. Hodges, Monazite-xenotime thermochronometry: Methodology and an example from the Nepalese Himalaya, *Contributions to Mineralogy and Petrology*, 141, 233-

247, 2001.

- Walker, C.B., M.P. Searle, and D.J. Waters, An integrated tectonothermal model for the evolution of the High Himalaya in western Zaskar with constraints from thermobarometry and metamorphic modeling, *Tectonics*, *20*, 810-833, 2001.
- White, N.M., M.S. Pringle, E. Garzanti, M.J. Bickle, Y.M.J. Najman, H. Chapman, and P. Friend, Constraints on the structural evolution, exhumation, and erosion of the High Himalayan Slab, NW India, from foreland basin deposits, *Earth and Planetary Science Letters*, *195*, 29-44, 2002.
- Willett, S.D., C. Beaumont, and P. Fullsack, Mechanical model for the tectonics of doubly vergent compressional orogens, *Geology*, *21*, 371-374, 1993.
- Wu, C., K.D. Nelson, G. Wortman, S.D. Samson, Y. Yue, J. Li., W.S.F. Kidd, and M.A. Edwards, Yadong cross structure and the South Tibetan Detachment in the east central Himalaya (89°-90°E), *Tectonics*, *17*, 28-45, 1998.
- Zeitler, P.K., P.O. Koons, M.P. Bishop, C.P. Chamberlain, D. Craw, M.A. Edwards, S. Hamidullah, M.Q. Jan, M.A. Khan, M.U.K. Khattak, W.S.F. Kidd, R.L. Mackie, A.S. Meltzer, S.K. Park, A. Pecher, M.A. Poage, G. Sarker, D.A. Schneider, L. Seeber, and J.F. Shroder, Crustal reworking at Nanga Parbat, Pakistan: Metamorphic consequences of thermal-mechanical coupling facilitated by erosion, *Tectonics*, *20*, 712-728, 2001.

Figure Captions

Figure 1. Initial conditions, model HT1. Only the central region of the model (600-1400 km) is shown here; full model width is 2000 km. Calculations are done on a finite element grid using the Arbitrary Lagrangian-Eulerian (ALE) method [Fullsack, 1995]. a) Passive marker grid and mechanical layers (light grey = middle crustal layer). Vertical markers numbered to facilitate comparison with deformed grids (Fig. 2); 0 = model 'suture'. b) Thermal layers (light grey = A_1 layer), initial isotherms (horizontal lines) calculated for conductive steady-state with $T_{surface} = 0^\circ\text{C}$ and $q_m = 20\text{ mW/m}^2$, and instantaneous velocity vectors (short dark lines). Subcrustal velocity vectors represent the effect of kinematic slab subduction at $V_P - V_S = 2.5\text{ cm/y}$ and slab advance at $V_S = 2.5\text{ cm/y}$. c) Relationship between mechanical and thermal layers and summary of parameters (see also Table 1). Surface denudation functions ($f(t)$, $g(x)$) are defined in Table 1; $f(x)$ is also plotted in Fig. 10a. d) Effect of linear reduction in viscosity from flow law value at 700°C to 10^{19} Pa.s at 750°C ('melt weakening'). Effective viscosity (η_{eff}) used in model shown by solid line, that predicted by flow law(s) shown schematically by dashed line. Further details in text, Table 1, and *Beaumont et al.* [2004].

Figure 2: Crustal-scale deformation and thermal evolution of model HT1 (V=H). For ease of presentation, all model results are shown in a fixed S-point reference frame [details in *Beaumont et al.*, 2004]. Upper panel in each set shows deformed marker grid and mechanical layers (grey = middle crustal layer); lower panel shows isotherms, velocity vectors, and thermal layers (grey = A_1 layer). Heavy dotted line represents position of model suture (vertical marker '0'). Also shown is spatial distribution and rate of slope-dependent erosion across the model surface; scale maximum = 1 cm/y . Panels a-d represent significant times in Himalayan metamorphic evolution: a) $21\text{ My} = 33\text{ Ma}$ (M1 or Eohimalayan metamorphism); b) $33\text{ My} = 21\text{ Ma}$ (M2 or

Neohimalayan metamorphism); c) 42 My = 12 Ma (onset of LHS metamorphism); d) 54 My = 0 Ma (present day). Results from the same model at different times are presented in *Beaumont et al.* [2004].

Figure 3: Crustal-scale distribution of model metamorphic facies and isotherms for times shown in Fig. 2. Facies constructed by comparing model T_{max} and $P@T_{max}$ values (interpreted as equivalent to peak metamorphic grade) to simplified metamorphic grid shown at bottom of diagram. Heavy dotted line shows position of model suture (see also Fig. 2). Panels a-b show close correspondence between isotherms and facies boundaries in early stages of model evolution; panels c-d show discordance between isotherms and facies boundaries below the erosion front resulting from efficient exhumation that begins at 24 My. Symbols in panels a-d show positions of two points (white = G1, Fig. 4; black = L3, Fig. 6), originally widely separated, that are juxtaposed at the erosion front at the end of the model (details in Fig. 4, 6, 8d); corresponding P - T - t paths are shown in the facies diagram. Animations can be viewed at http://geodynam.ocean.dal.ca/jgr/test54_1.gif and [test54_2.gif](http://geodynam.ocean.dal.ca/jgr/test54_2.gif).

Figure 4: Results from model HT1 for tracked "GHS" points that emerge together above "MCT" at end of model; pairs of points shown on separate panels for clarity. Initial positions (x,z) in km: G1 = 400, 15.6; G2 = 330, 10.0; G3 = 330, 7.5; G4 = 330, 5.0. Symbols at 6 My intervals. a) Particle (x - z) paths show transport of points into orogen, burial during crustal thickening, reversal of transport direction corresponding to onset of channel flow, lateral translation in channel, and exhumation at erosion front. Horizontal scale is distance from edge of model grid; vertical scale is depth below model surface; surface elevation changes with time and is not shown. Positions and times of tracked points at T_{max} and P_{max} also shown. b) P - T paths for same points. Reaction boundaries shown for reference: KA: kyanite = andalusite; AS: andalusite

= sillimanite [*Holdaway*, 1971; alternative boundary shown in Fig. 5]; KS: kyanite = sillimanite; MQ: muscovite + quartz = Al_2SiO_5 + K-feldspar + H_2O ; WM: fluid-present melting of granitoid rocks. c) Depth-time ($z-t$) and temperature-time ($T-t$) paths, plotted on same panels to facilitate comparison between exhumation (upper) and cooling (lower) histories. Depth scale on upper right; temperature scale on lower left.

Figure 5: Comparison between model $P-T-t$ results for "GHS" and data from GHS. a) Model $P-T$ paths (grey lines, G1-G3) compared with $P-T$ paths constructed from zoned garnets from various localities [VG98 = isobaric heating path, *Vannay and Grasemann*, 1998; VM98, W01 = steep prograde paths, *Vance and Mahar*, 1998; *Walker et al.*, 2001; H93 = isothermal decompression paths, *Hodges et al.*, 1993; C90 = *Craw*, 1990]. Al_2SiO_5 phase diagram shown for reference [H71 = andalusite-sillimanite boundary, *Holdaway*, 1971; P92 = same boundary, modified by *Pattison*, 1992]. b) Model $T-t$ paths (grey lines, G1-G3) compared with data from Nepal and adjacent southern Tibet [S97, S99 = *Searle et al.*, 1997, 1999a; C98 = *Coleman*, 1998; C91 = *Copeland et al.*, 1991; C01 = *Catlos et al.*, 2001].

Figure 6: Results from model HT1 for tracked "LHS" points that emerge together below "MCT" at end of model; pairs of points shown on separate panels for clarity. Initial point positions (x,z) in km: L1 = -950, 7.5; L2 = -940, 8.1; L3 = -750, 18.1; L4 = -520, 16.9 (all to the left of the region shown in panel a). Symbols at 6 My intervals. a) Particle ($x-z$) paths show transport of points into orogen, burial beneath advancing orogenic front, and exhumation below the "MCT" as orogen propagates into its foreland. Positions and times of tracked points at T_{max} and P_{max} also shown. b) $P-T$ paths for same points; reaction boundaries as in Fig. 4. c) Depth-time ($z-t$) and temperature-time ($T-t$) paths, note similarities in exhumation and cooling paths, in contrast to "GHS" points (Fig. 4c).

Figure 7: Comparison between model P - T - t results for "LHS" and data from LHS of central Nepal. a) Model P - T paths (grey lines, L2-L4) compared with P - T paths constructed from zoned garnets, Darondi section, central Nepal [K01 = *Kohn et al.*, 2001]. Al_2SiO_5 phase diagram as in Fig. 5. b) Model T - t paths (grey lines, L2-L4) compared with data from central Nepal [C91 = $^{40}\text{Ar}/^{39}\text{Ar}$ hornblende and biotite ages, *Copeland et al.*, 1991; C01 = U-Pb monazite and $^{40}\text{Ar}/^{39}\text{Ar}$ muscovite ages, *Catlos et al.*, 2001].

Figure 8: Model peak grade profiles compared with data from central Nepal. a) Model T_{max} (open circles) vs. metamorphic peak T data (filled points with error bars) from the Langtang region. [IH92 = *Inger and Harris*, 1992; M95 = *Macfarlane*, 1995; F00 = *Fraser et al.*, 2000]. b) Model $P@T_{max}$ (open squares) vs. metamorphic P data (filled points with error bars) from the Langtang region. c) Model age profiles (open symbols) vs. monazite (U-Th-Pb) and muscovite ($^{40}\text{Ar}/^{39}\text{Ar}$) data (filled points) from Marsyandi-Darondi region [C01 = *Catlos et al.*, 2001]. $t@T_{max}$ = model time of T_{max} ; t_{700} , t_{500} , t_{350} = model times of cooling through 700°C, 500°C, 350°C respectively; these values can be interpreted as cooling or growth ages by comparison with the T_{max} profile in (a). Arrows marked "ages not reset" indicate low T_{max} regions where model ages do not reflect tectonics. d) Tectonic and thermal configuration of model HT1 in the vicinity of the erosion front at 54 My (0 Ma); horizontal scale as for upper panels (V=H). Note that superimposed particle paths for tracked points ("LHS" = dashed lines; "GHS" = solid lines) span longer time range. Positions of tracked points at 6 Ma ("LHS" - open circles; "GHS" - open squares) illustrate relative displacement and tectonic juxtaposition in last 6 My of model evolution; full particle paths and P - T - t data are shown in Fig. 4 (G1-G4) and Fig. 6 (L1-L4). See text and Table 2 for discussion of correspondence between model features ("MCT", "GHS", etc.) and observed Himalayan features.

Figure 9: Observed radiometric ages from Himalaya of Nepal (a) compared with times recorded by points at surface at end of model HT1 (b). M1 and M2 represent times of Eohimalayan and Neohimalayan metamorphism, respectively. Further discussion in text. Data sources: *Schärer*, [1984]; *Schärer et al.* [1986]; *Copeland et al.* [1991]; *Harrison et al.* [1995, 1997, 1999]; *Hodges et al.* [1996]; *Vannay and Hodges* [1996]; *Coleman* [1998]; *Grove and Harrison* [1999]; *Searle et al.*, [1999a]; *Simpson et al.* [2000]; *Godin et al.* [2001]; *Catlos et al.* [2001].

Figure 10. a) Relative value of temporal erosion function ($f(t)$) compared with maximum model response (slope $\times f(t) \times g(x)$) in regions of highest surface slope (details in Fig. 2). Relative rates: H = high; M = moderate; L = low; maximum rate ca. 1 cm/y. b) Eroded model facies (grey regions) compared with observed detrital minerals (solid and open symbols) in Himalayan foreland basin deposits. For model results, shaded regions show relative proportion of model facies at the surface in the region undergoing denudation at that time (Fig. 3); vertical bars show maximum % for each facies. Facies boundaries as in Fig. 3, except that here "sub-greenschist" includes both "sub-metamorphic" and "blueschist". Relative metamorphic grade: H = high; M = medium; L = low. Discussion in text. Data sources: *DeCelles et al.* [1998]; *Najman and Garzanti* [2000]; *White et al.* [2002]; *Najman et al.* [2002]; grouping of staurolite, kyanite, and sillimanite reflects different ways of reporting data.

Figure 11. Model results relevant to lower crustal metamorphism (granulite and eclogite facies). a) P - T paths for tracked points E1, E2, lying at mid-crustal depths at the end of the model. Path segment a = crustal thickening stage; b = maximum burial (eclogite facies conditions); c = entrainment in channel flow (granulite facies conditions). Shaded region represents the transition zone from plagioclase-bearing to plagioclase-free assemblages via the reaction albite (ab) =

jadeite (jd) + quartz (qz); other reaction boundaries as in Fig. 4. b) Corresponding particle paths; 40 km reference line shows approximate position of surface following prolonged post-orogenic denudation. Surface position of model "MCT" shown for reference. c) Dynamic pressure (P_{dyn}) including the effects of both burial depth and tectonic stress vs. lithostatic pressure (P_{lith}) for point E2; similar results are obtained from all other tracked points in the model.

Figure 12: Comparison of some previous models for Himalayan metamorphism and exhumation (a-d) with channel flow model HT1 (e). a) Inverted metamorphism resulting from heating by hot upper plate [e.g., *LeFort, 1975; Hollister, 1993; Royden, 1993*]. b) Inverted metamorphism resulting from frictional heating along the MCT [e.g., *Molnar and England, 1990; Harrison et al., 1998*]. c) Inverted metamorphism in MCT zone and normal metamorphism in GHS resulting from deformation of pre-existing metamorphic sequence, represented schematically by the kyanite (ky) isograd [e.g., *Searle and Rex, 1989; Hubbard, 1996*]. d) Inverted and normal metamorphism resulting from distributed ductile deformation and associated velocity gradient (arrows) accompanying extrusion of crustal wedge [e.g., *Hodges et al., 1993, 1996; Grujic et al., 1996; Vannay and Grasemann, 2001*]. e) Essential features of channel flow model, as discussed in text. Simplified particle and P - T paths shown for points successively incorporated into growing orogen (A enters orogen first, C enters last). Solid lines (A, B) represent "GHS" material; dashed line (C) represents "LHS" material.

Table 1. Parameters used in model HT1 (see also Figure 1).

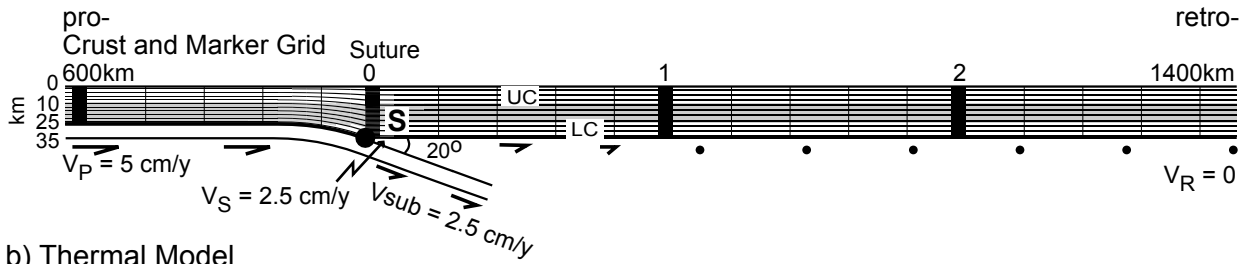
Parameter	Meaning	Value(s)
a) Mechanical parameters		
V_P	pro-side (convergence) velocity	5 cm/y
V_R	retro-side velocity	0 cm/y
V_S	S-point velocity (subduction advance)	2.5 cm/y
θ	subduction dip angle	20°
D	flexural rigidity (isostasy model)	10 ²² Nm
ρ_{crust}	crustal density	2700 kg/m ³
ρ_{mantle}	mantle density	3300 kg/m ³
ϕ_{eff}	effective internal angle of friction	5° (0-10 km) 15° (10-35 km)
$\eta_{eff}^v = B^* \cdot (\dot{I}_2)^{(1-n)/2n} \cdot \exp[Q/nRT_K]$	general equation for effective viscosity	
\dot{I}_2	second invariant of strain rate tensor	s ⁻²
R	gas constant	8.314 J/mol°K
T_K	absolute temperature	°K
WQ (0-10 km)	wet Black Hills quartzite flow law [after <i>Gleason and Tullis</i> , 1995]	$n = 4.0$ $B^* = 2.92 \times 10^6 \text{ Pa}\cdot\text{s}^{1/4}$ $Q = 223 \text{ kJ/mol}$
WQ x 5 (10-25 km)	modified wet Black Hills quartzite flow law	$B^* = B^*(\text{WQ}) \times 5$ n, Q as above
DMD (25-35 km)	dry Maryland diabase flow law [after <i>Mackwell et al.</i> , 1998]	$n = 4.7$ $Q = 485 \text{ kJ/mol}$ $B^* = 1.91 \times 10^5 \text{ Pa}\cdot\text{s}^{1/4.7}$
'melt weakening' (WQ and WQ x 5 only)	linear reduction in effective viscosity over T range 700-750°C	η_{700} = flow law value $\eta_{750} = 10^{19} \text{ Pa}\cdot\text{s}$
b) Thermal parameters		
$\rho C_p(\partial T/\partial t + \underline{v} \cdot \nabla T) = K\nabla^2 T + A$	heat balance equation	
\underline{v}	tectonic velocity field	
K	thermal conductivity	2.00 W/m°K
C_p	heat capacity	
κ	thermal diffusivity ($\kappa = K/\rho C_p$, where $\rho C_p = 2 \times 10^6$)	1.0 x 10 ⁻⁶ m ² /s
T_a	temperature at lithosphere/ asthenosphere boundary	1350°C
q_m	basal mantle heat flux	20 mW/m ²
q_s	initial surface heat flux	71.25 mW/m ²
A_1 (0-20 km)	upper crustal heat production	2.0 $\mu\text{W/m}^3$
A_2 (20-35 km)	lower crustal heat production	0.75 $\mu\text{W/m}^3$
c) Surface denudation		
$\dot{e} = \text{slope} \times f(t) \times g(x)$	denudation rate (m/y)	

slope	local surface slope	
$f(t)$	time function	
	specifies how denudation rate (m/y) varies with time when $g(x)$ and slope = 1	
$g(x)$	spatial function	
	specifies how denudation rate varies with position x	$g(x) = 0 = \text{arid}$ $g(x) = 1 = \text{wet}$
$f(t)$		
	varies linearly	0.0 $t \leq 24 \text{ My}$
		0.0 \rightarrow 0.133 m/y $24 < t < 27 \text{ My}$
	*	0.133 m/y $27 \leq t \leq 39 \text{ My}$
	varies linearly	0.133 \rightarrow 0.04 m/y $39 < t < 48 \text{ My}$
		0.04 m/y $48 \leq t \leq 54 \text{ My}$
	* gives denudation rate of 1.33 cm/y where slope = 1:10 and $g(x) = 1.0$	
$g(x)$		
	varies linearly	1.0 $0 < x \leq 500 \text{ km}$
		1.0 \rightarrow 0.0 $500 < x < 550 \text{ km}$
		0.0 $x \geq 550 \text{ km}$

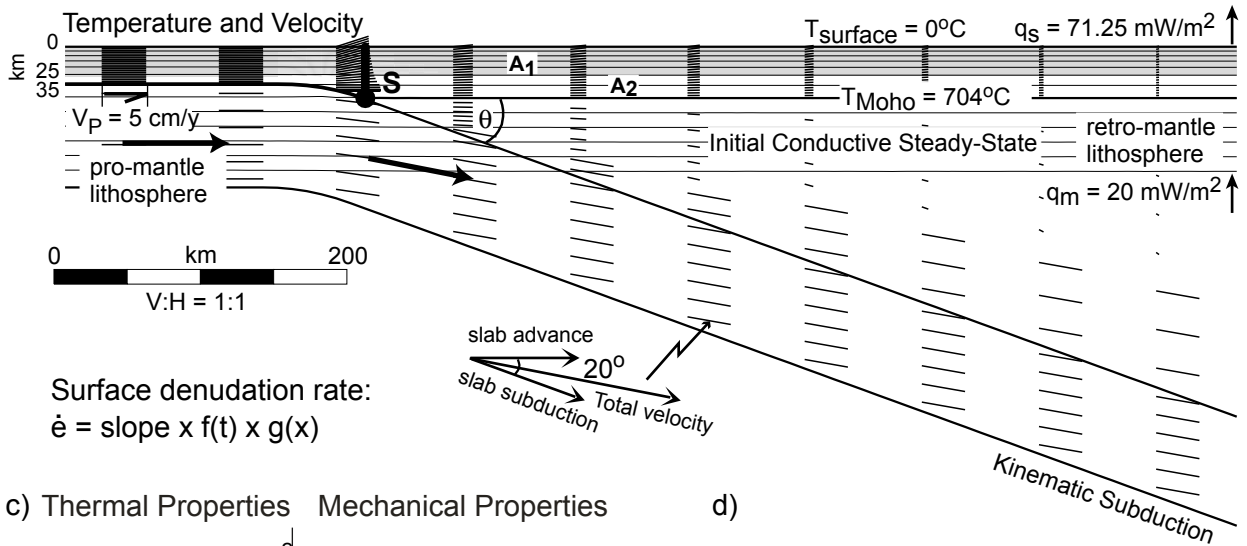
Table 2. Notation used for comparing model results with data from the Himalayan-Tibetan system.

Notation	Meaning in model HT1	Equivalent in nature
My	millions of years since start of model	interval of millions of years
Ma	millions of years before end of model (end of model = 54 My; Ma = 54-My)	millions of years before present
"MCT"	protolith boundary between extruded channel material and newly accreted pro-crust	MCT = Main Central Thrust zone
"STD"	upper boundary of channel ($T_{\max} \geq 700^{\circ}\text{C}$ in channel)	STD = South Tibetan Detachment system
"LHS"	deformed material below "MCT"	LHS = Lesser Himalayan Sequence
"GHS"	extruded channel and overlying exhumed middle crust ($T_{\max} \geq 350^{\circ}\text{C}$)	GHS = Greater Himalayan Sequence
"TS"	cooler, less deformed upper crust above exhumed middle crust	TS = Tethyan series
"suture"	boundary between pro- and retro-crust (marker 0, Figs. 1, 2)	Indus-Tsangpo suture

a) Mechanical Model

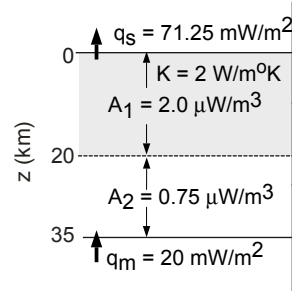


b) Thermal Model

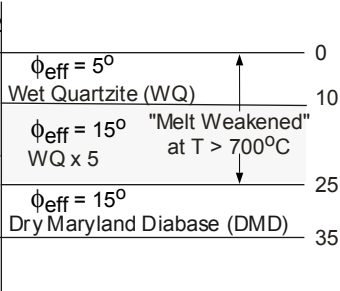


Surface denudation rate:
 $\dot{\epsilon} = \text{slope} \times f(t) \times g(x)$

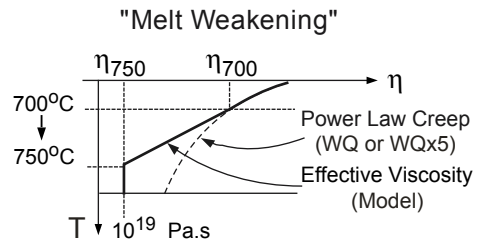
c) Thermal Properties



Mechanical Properties



d)



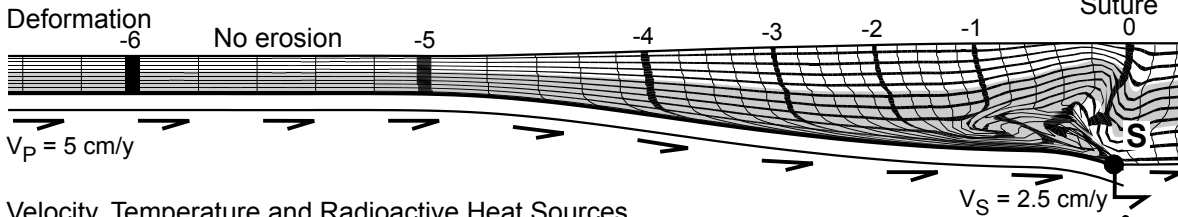
Jamieson et al., FIGURE 1

Model HT1

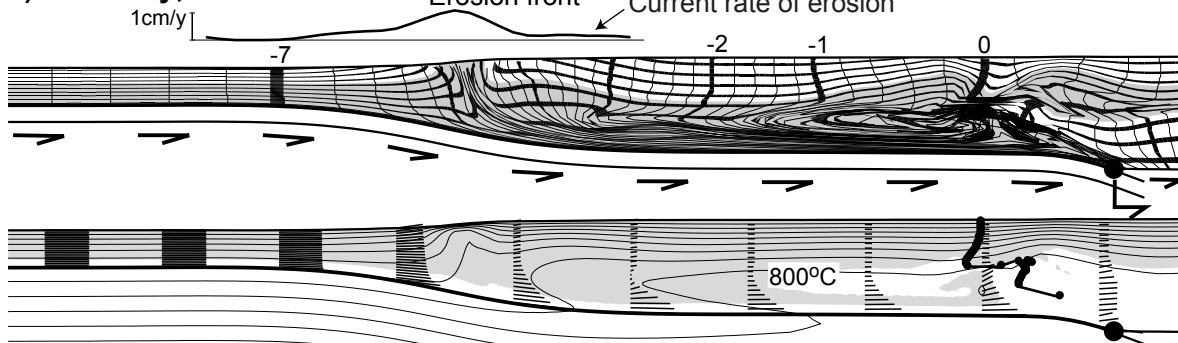
pro-

retro-

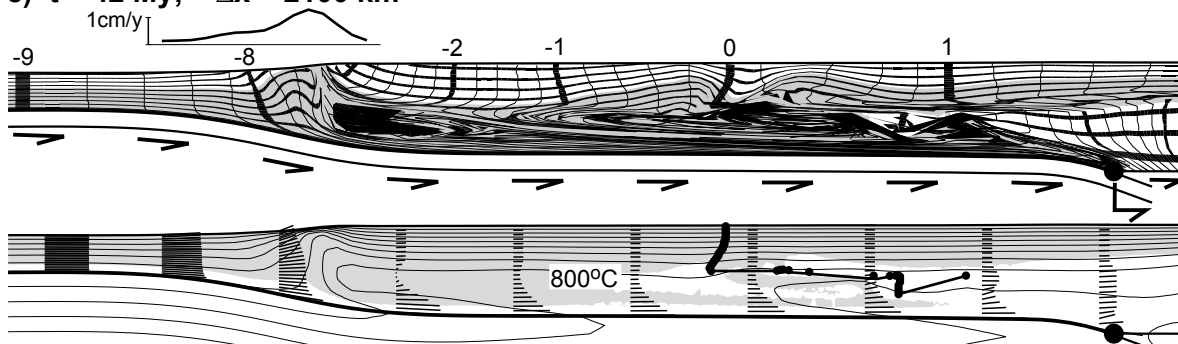
a) $t = 21$ My; $\Delta x = 1050$ km



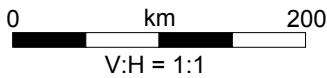
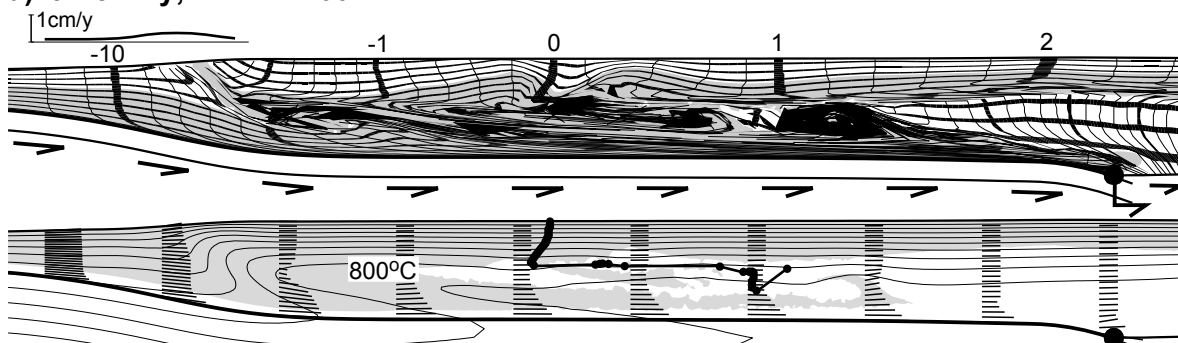
b) $t = 33$ My; $\Delta x = 1650$ km



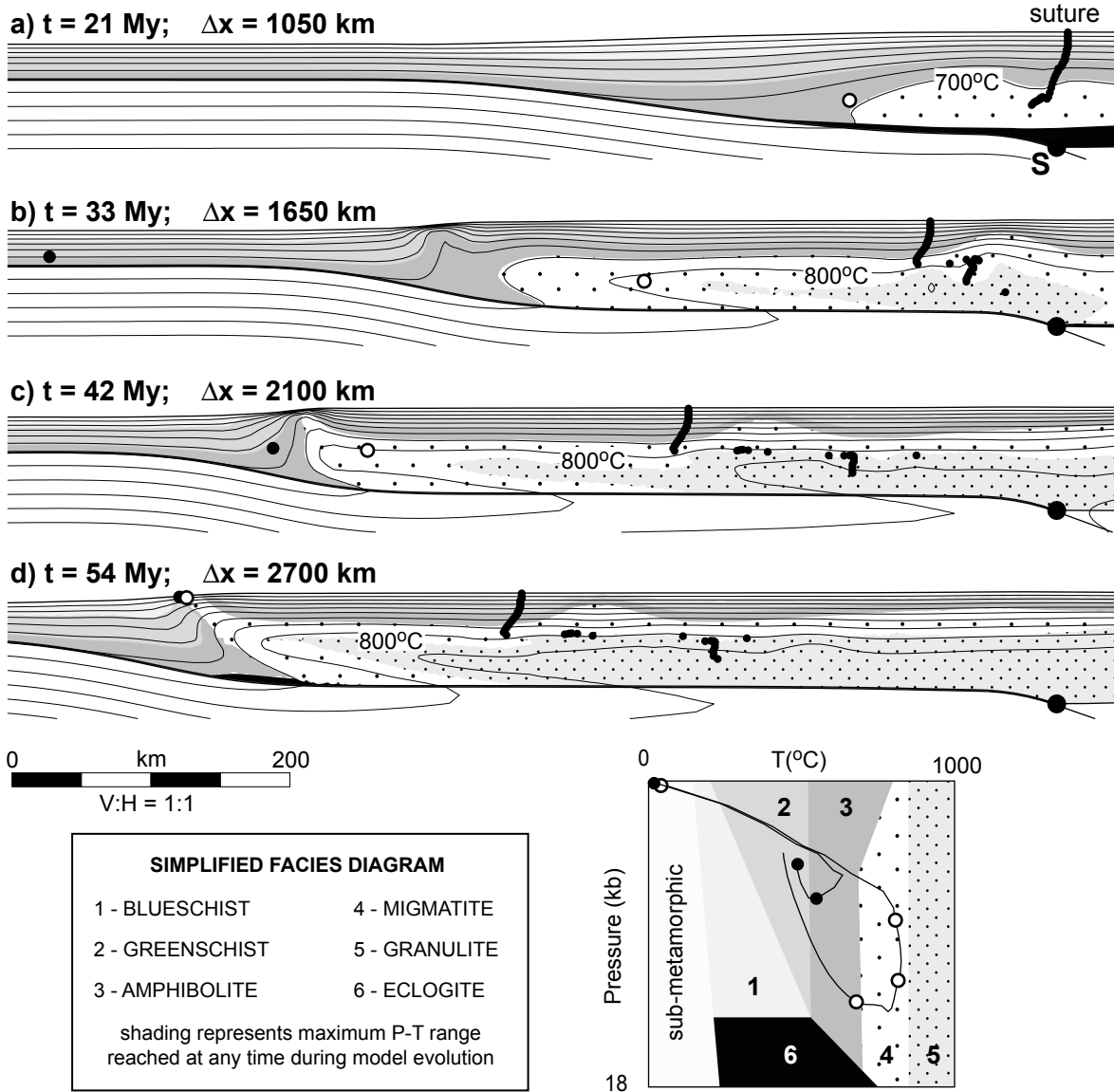
c) $t = 42$ My; $\Delta x = 2100$ km



d) $t = 54$ My; $\Delta x = 2700$ km



Jamieson et al., FIGURE 2

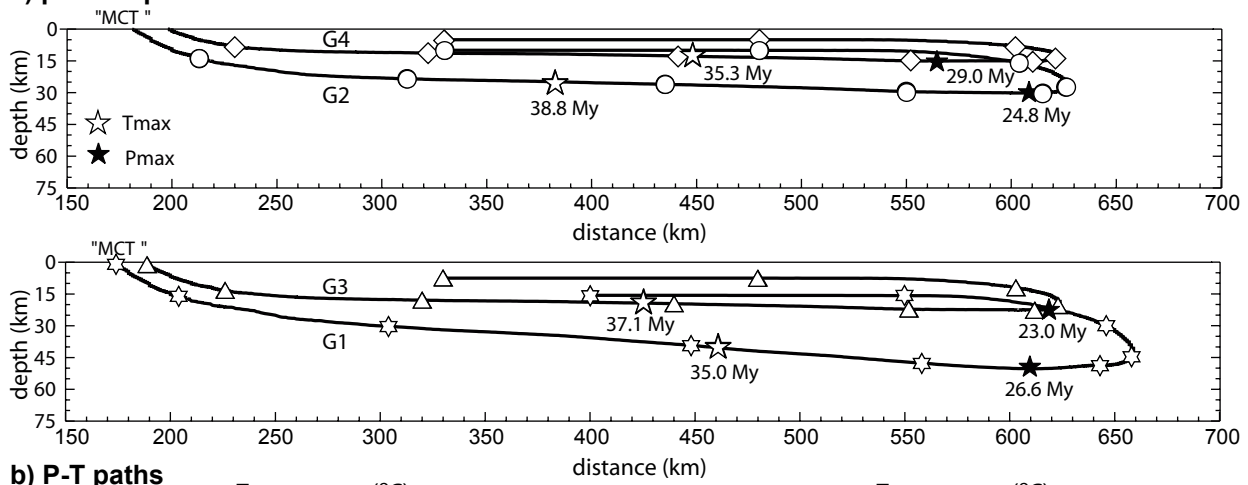


Jamieson et al., FIGURE 3

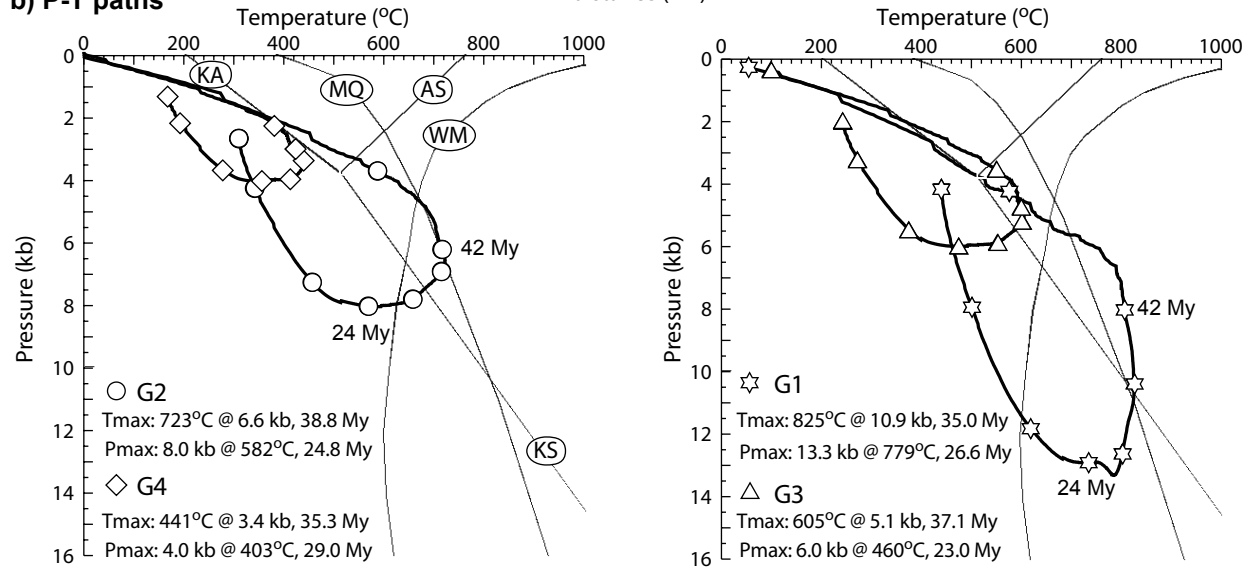
MODEL HT1: "GHS" PTt results

a) particle paths

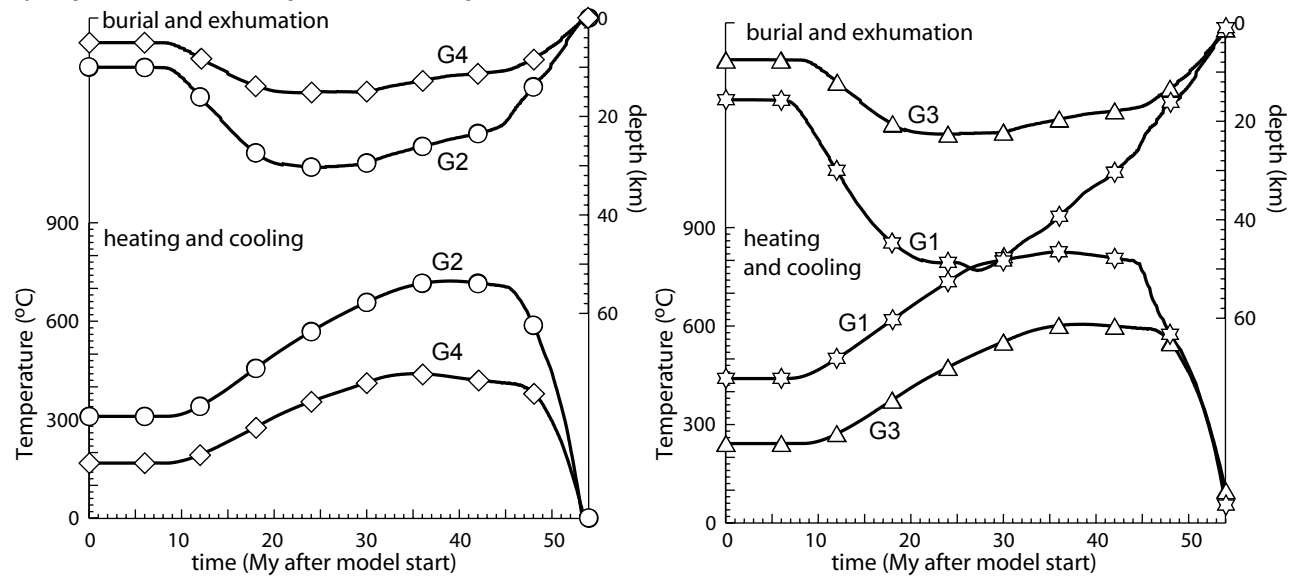
times in My after model start; symbols at 6 My intervals

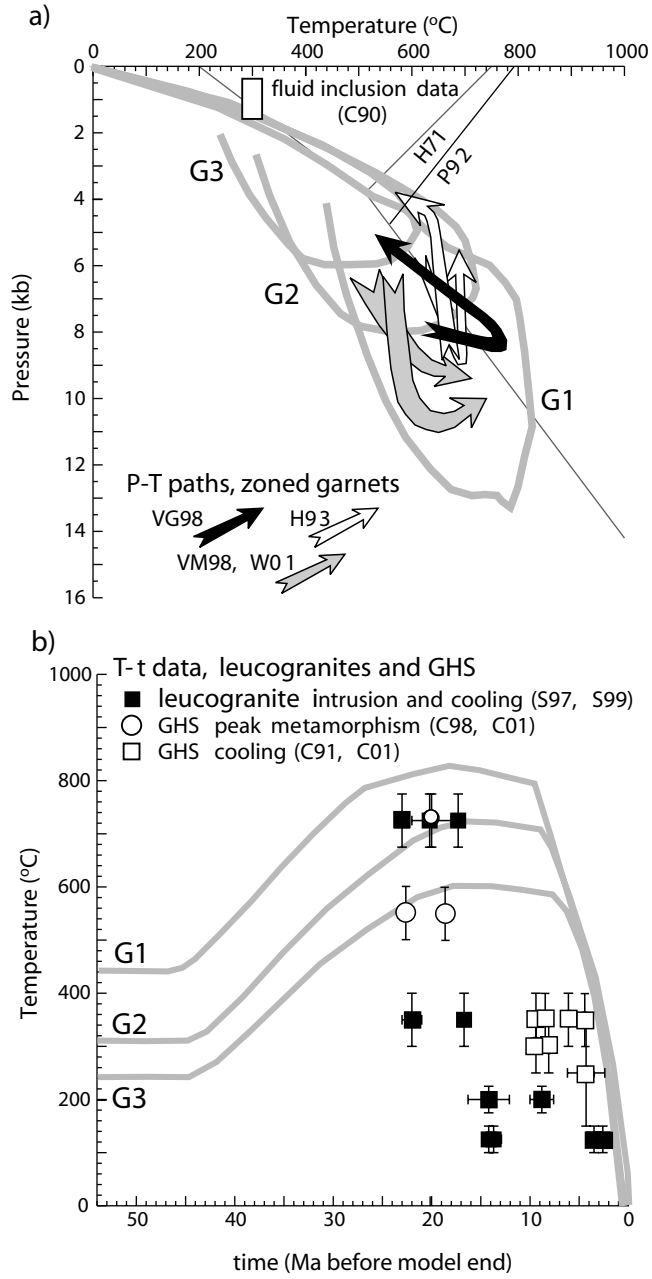


b) P-T paths



c) depth-time and temperature-time paths



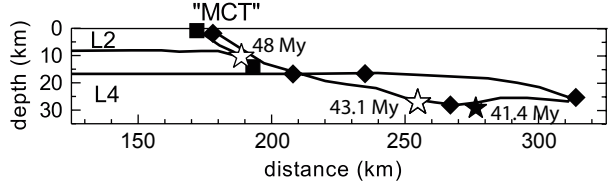
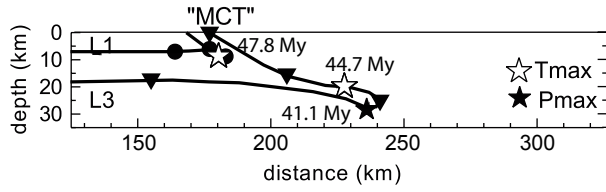


Jamieson et al., FIGURE 5

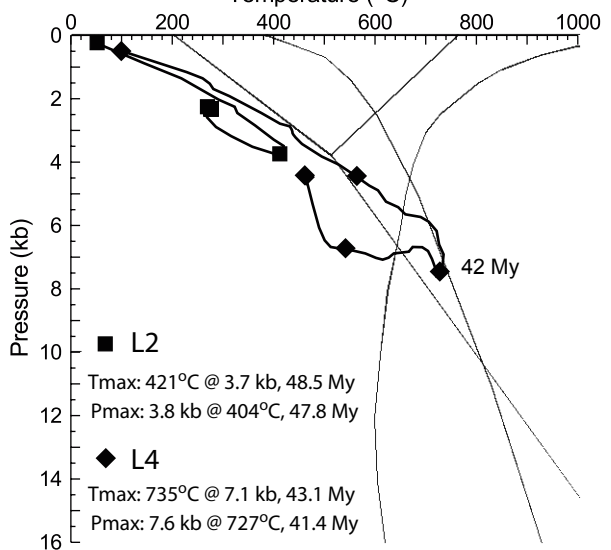
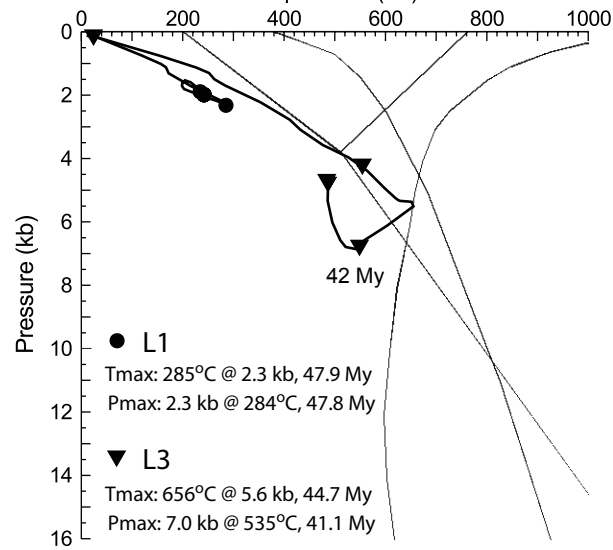
MODEL HT1: "LHS" PTt results

times in My after model start; symbols at 6 My intervals

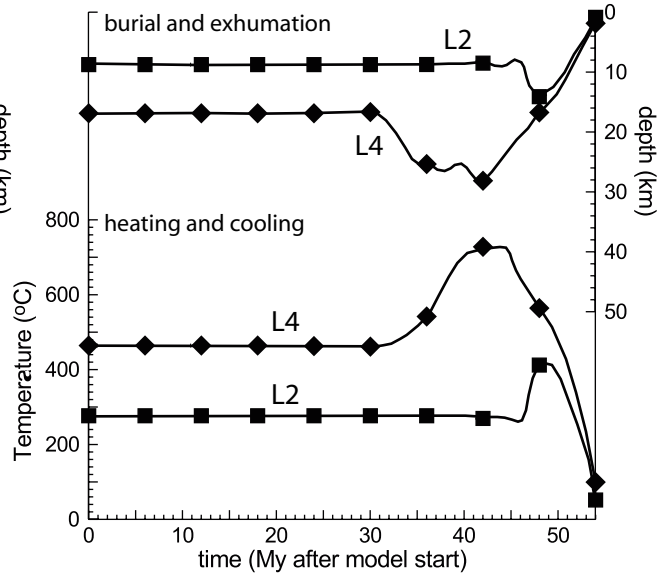
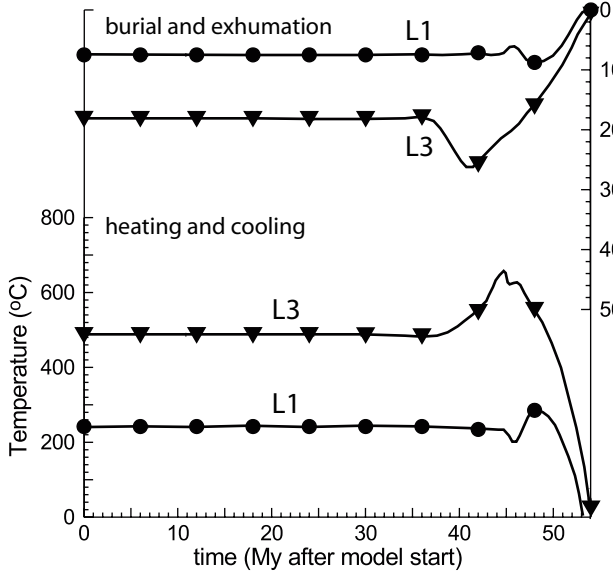
a) particle paths

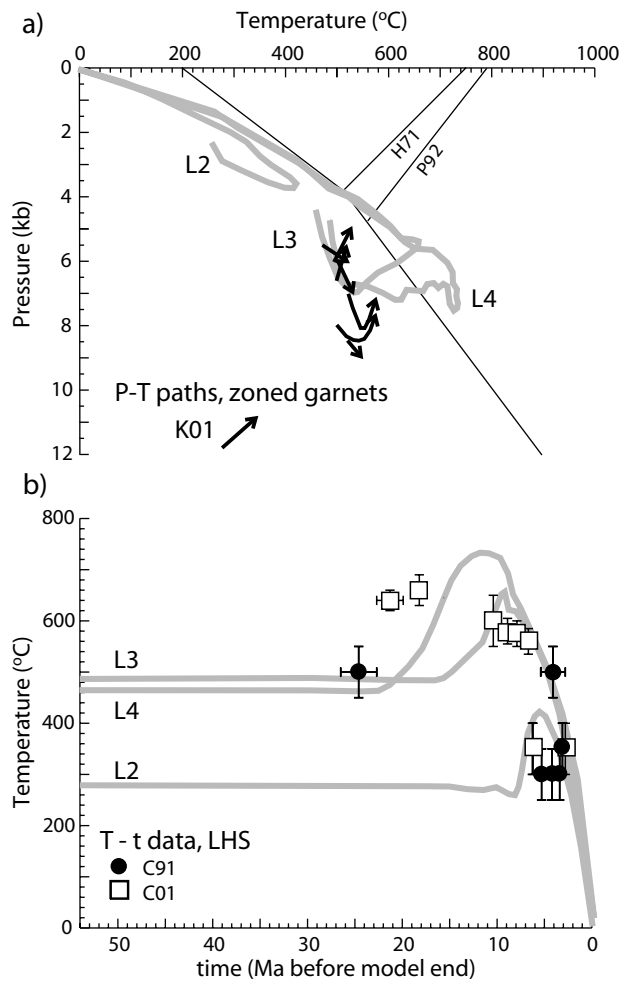


b) P-T paths

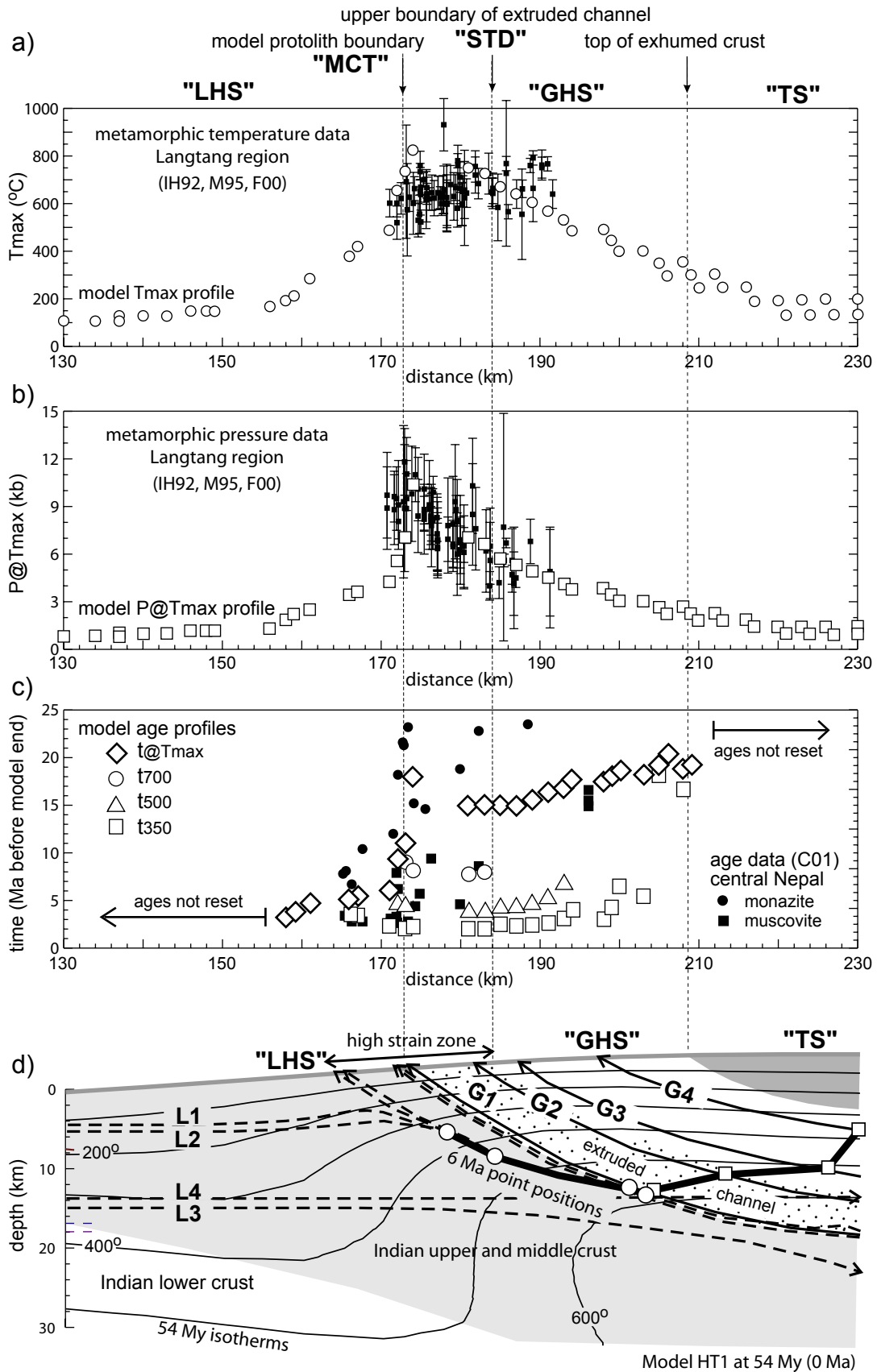


c) depth-time and temperature-time paths

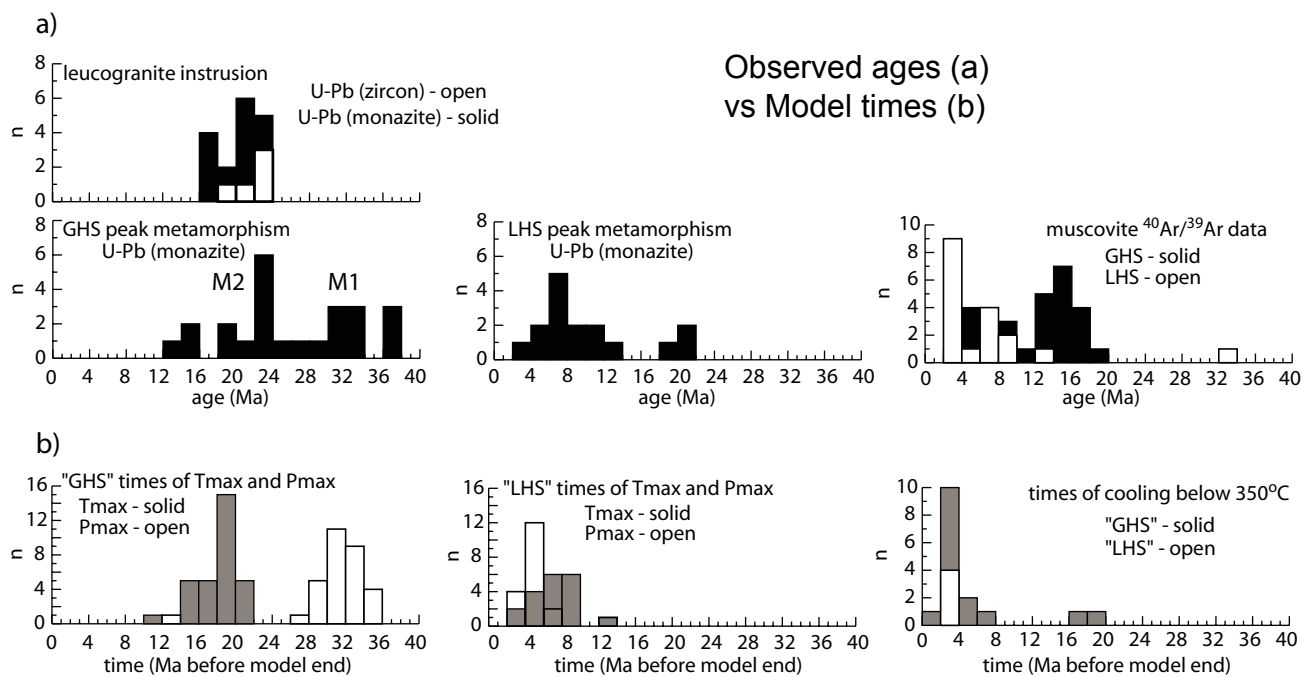




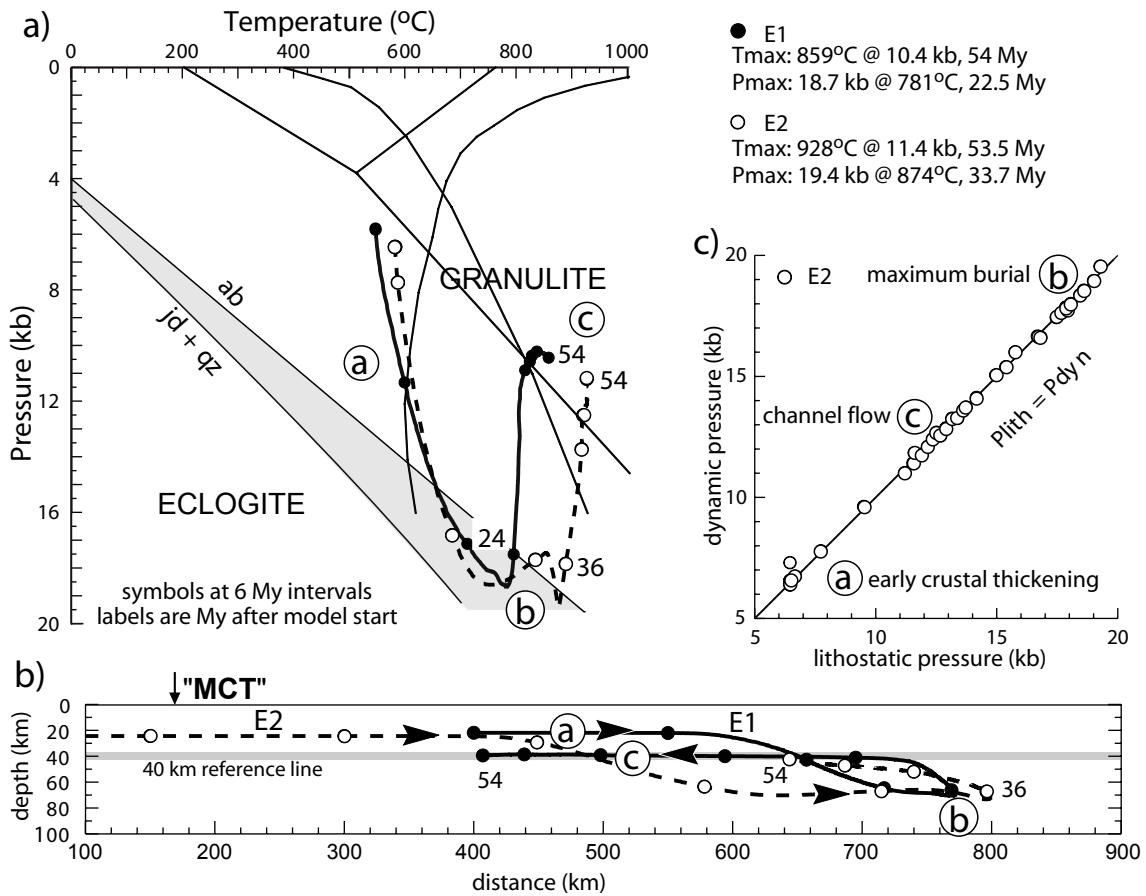
Jamieson et al., FIGURE 7



Jamieson et al., FIGURE 8



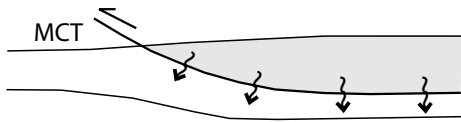
Jamieson et al., FIGURE 9



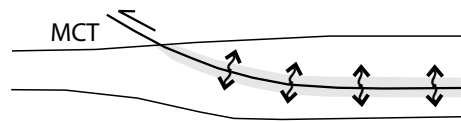
Jamieson et al., FIGURE 11

Models of Himalayan metamorphism and exhumation

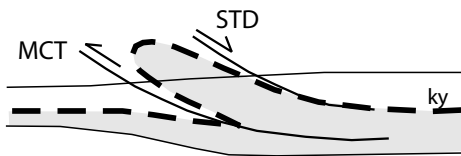
a) hot upper plate



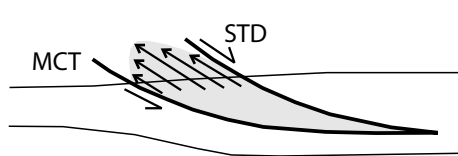
b) frictional heat



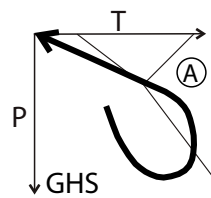
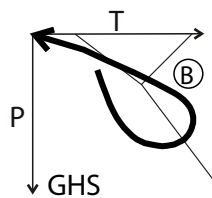
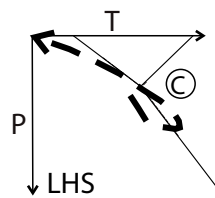
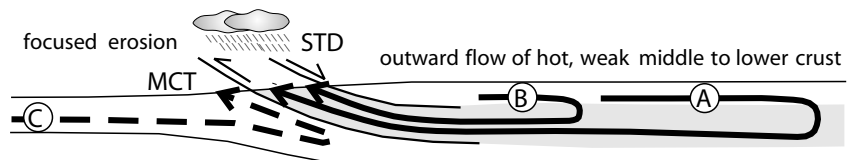
c) deformation of isograds



d) extrusion of wedge



e) channel flow (this study)



Jamieson et al., FIGURE 12